

# Salient Objects in Clutter

Deng-Ping Fan, Jing Zhang, Gang Xu, Ming-Ming Cheng, and Ling Shao, *Fellow, IEEE*

**Abstract**—In this paper, we identify and address a serious design bias of existing salient object detection (SOD) datasets, which unrealistically assume that each image should contain at least one clear and uncluttered salient object. This *design bias* has led to a saturation in performance for state-of-the-art SOD models when evaluated on existing datasets. However, these models are still far from satisfactory when applied to real-world scenes. Based on our analyses, we propose a new high-quality dataset and update the previous saliency benchmark. Specifically, our dataset, called Salient Objects in Clutter (**SOC**), includes images with both salient and non-salient objects from several common object categories. In addition to object category annotations, each salient image is accompanied by attributes that reflect common challenges in real-world scenes, which can help provide deeper insight into the SOD problem. Further, with a given saliency encoder, *e.g.*, the backbone network, existing saliency models are designed to achieve mapping from the training image set to the training ground-truth set. We therefore argue that improving the dataset can yield higher performance gains than focusing only on the decoder design. With this in mind, we investigate several dataset-enhancement strategies, including label smoothing to implicitly emphasize salient boundaries, random image augmentation to adapt saliency models to various scenarios, and self-supervised learning as a regularization strategy to learn from small datasets. Our extensive results demonstrate the effectiveness of these tricks. We also provide a comprehensive benchmark for SOD, which can be found in our repository: <http://dpfan.net/SOCBenchmark>.

**Index Terms**—Salient object detection, SOD, SOC, survey, dataset, benchmark.

## 1 INTRODUCTION

THIS paper considers the task of salient object detection (SOD), which aims to detect the most attention-grabbing objects in a scene and then extract pixel-accurate silhouettes for them. The merit of SOD lies in its many applications, including foreground map evaluation [2], [3], [4], visual tracking [5], [6], [7], action recognition [8], image retrieval [9], [10], information discovery [11], [12], image contrast enhancement [13], person re-identification [14] image segmentation [15], [16], video segmentation [17], photo synthesis [18], content-aware image editing [19], image caption [20], and video compression [21], [22], style transfer [23], [24], image matching [25], autonomous underwater robots [26], camouflaged object detection [27], aesthetic scoring [28], self-driving vehicles [29], plant species identification [30], VR/AR [31]<sup>1</sup>, Sony’s BRAVIA XR TV<sup>2</sup>, *etc.* However, existing SOD datasets [32], [33], [34], [35], [36], [37], [38], [39], [40], [41], [42] are flawed either in their data collection procedure or data quality. Specifically, most datasets assume that an image should contain at least *one salient object*, and thus they discard images that do not contain any salient objects. We call this **DATA SELECTION BIAS** [43].

Moreover, existing datasets typically contain images with a single object or several uncluttered objects. These datasets do not adequately reflect the complexity of real-world images, where scenes usually contain multiple objects amidst significant clutter. As a result, all top-performing models trained on the existing large-



Figure 1. Examples from our new SOC dataset, including *non-salient* (first row) and *salient* object images (rows 2 to 4). For salient object images, an instance-level ground-truth map (different color), object attributes (Attr) and category labels are provided.

scale datasets (*e.g.*, DUTS [41]) have nearly saturated performance (*e.g.*, SCRN [44] has an *S-measure* > 0.9 on ECSSD [37]), but still achieve unsatisfactory results on realistic images (*e.g.*, *S-measure* < 0.8 on SOC [1]). As the current SOD models are biased towards ideal conditions, their effectiveness may be impaired once they are applied to real-world scenes. To solve this problem, it is important to introduce a dataset with more realistic conditions.

Another issue faced by the RGB SOD community is that only the overall performance of the models can be analyzed using existing datasets. This is because none of the datasets contain attributes that reflect different real-world challenges. Having such attributes would help i) provide deeper insight into the SOD problem, ii) enable the pros and cons of the SOD models to

- Deng-Ping Fan, Gang Xu and Ming-Ming Cheng are with the CS, Nankai University, Tianjin, China. (E-mail: dengpfan@gmail.com; gangxu@mail.nankai.edu.cn; cmm@nankai.edu.cn)
- Jing Zhang is with Research School of Engineering, the Australian National University, ACRV, DATA61-CSIRO. (Email: zjnwpu@gmail.com)
- Ling Shao is with the Inception Institute of Artificial Intelligence, Abu Dhabi, UAE. (E-mail: ling.shao@inceptioniai.org)
- A preliminary version of this work appeared in ECCV [1].
- The major part of this work was done in Nankai University.
- Ming-Ming Cheng is the corresponding author.

1. AR CUT & PASTE: <https://www.youtube.com/watch?v=-N-podTAY9Y>.
2. <https://www.youtube.com/watch?v=4LnCuTAIVno&feature=youtu.be>.

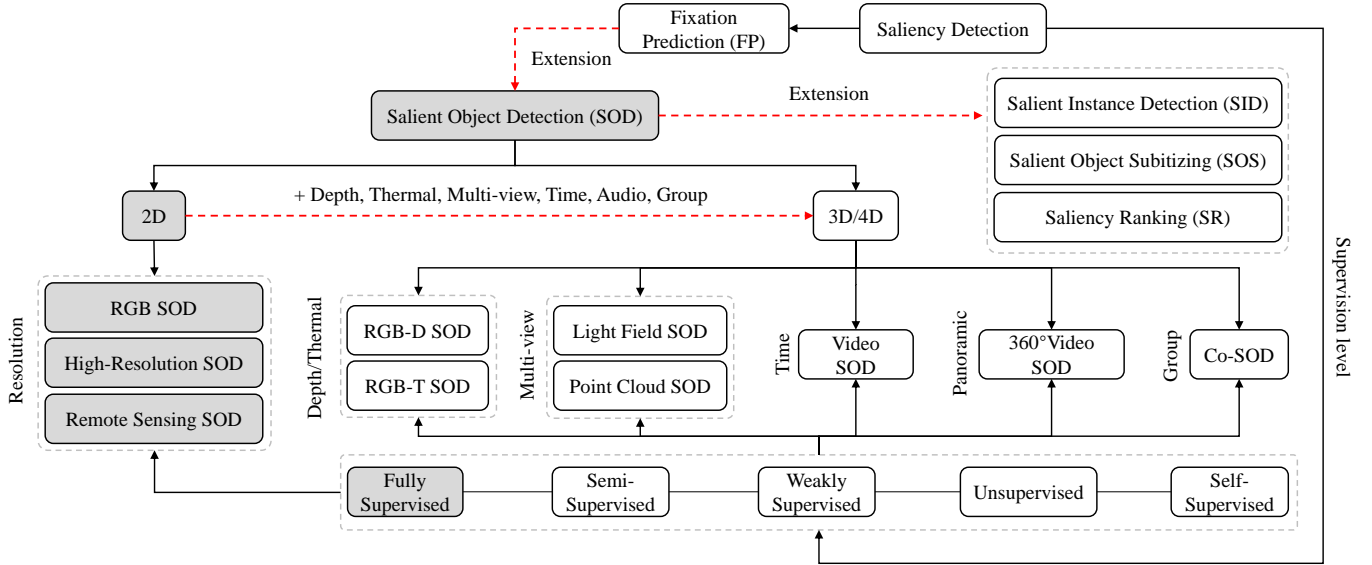


Figure 2. Taxonomy of the saliency detection task. We highlight the scope of this study in gray. See § 2 for details.

be investigated, and iii) allow the model performances to be objectively assessed from different perspectives. Finally, with a given saliency encoder, *e.g.*, the backbone network, existing saliency models are designed to achieve mapping from the training image set to the training ground-truth set. We thus argue that efforts on improving the dataset, *e.g.*, fixing the data bias issue, can yield higher performance gains than focusing only on the decoder design. Towards this, we investigate several dataset-enhancement strategies, including label smoothing to highlight salient boundaries, random image augmentation to adapt saliency models to various scenarios, and self-supervised learning as a form of regularization to learn from small datasets. Extensive experiments validate the effectiveness of these tricks.

Our contributions are summarized as follows:

- 1) **Dataset.** We collect a new high-quality SOD dataset, named “Salient Objects in Clutter,” or **SOC**. *SOC* is the largest instance-level SOD dataset to date, containing 6,000 images from more than 80 common categories. It differs from existing datasets in three aspects: i) Salient objects have category annotations, which can be used for new research problems, such as weakly supervised SOD. ii) The inclusion of non-salient images and objects makes this dataset more realistic and challenging than the existing ones. iii) Salient objects have attributes that reflect various situations encountered in the real world, such as *motion blur*, *occlusion* and *background clutter*. As a consequence, *SOC* narrows the gap between existing datasets and real-world scenes.
- 2) **Review & Benchmark.** We present the largest scale RGB SOD study, reviewing **201** representative models including **84** algorithms using handcrafted features and **117** deep learning based models. Besides, we also maintain an online benchmark (*i.e.*, <http://dpfan.net/SOCBenchmark>.) to dynamically trace the development of this field. In addition, we provide the most comprehensive benchmark of the **top-100** SOD models. To evaluate the models, for the first time, we not only present the overall but also an attribute-based performance evaluation. This allows a deeper understanding of the models and provides a more complete benchmark.

- 3) **Strategy.** We investigate the biased dataset issue and introduce three dataset-enhancement strategies; namely, label smoothing to make the model aware of the salient boundaries, random image augmentation to adapt the saliency models to various real-world scenarios, and self-supervised learning as a regularization technique to learn from small datasets. Despite the apparent simplicity of our strategies, we can achieve an average absolute improvement of 1.1%  $S_\alpha$  over five existing cutting-edge models.

- 4) **Discussions & Future Directions.** Based on our *SOC*, we present the pros and cons of the current SOD algorithms, discuss several under-investigated open issues, and provide potential future directions at six levels, *e.g.*, the dataset level, task level, model level, supervision level, evaluation level, and application level.

This work extends our previous conference version [1] in the following aspects. First, we provide more details on our *SOC*, including sample images without salient objects, images with attributes, and statistics of the attributes. Second, we study three novel training dataset related strategies to fully utilize the non-salient object data and achieve the new state-of-the-art performance. Third, we conduct the largest-scale (46 traditional and 54 deep learning models) benchmarking of SOD models on our *SOC*. Finally, based on our benchmarking results, we highlight several fundamental research directions and challenges in the SOD.

## 2 RELATED WORK

### 2.1 Scope

Salient object detection originated from the task of fixation prediction (FP) [45], [46], switching attention regions for accurate object-level regions. SOD can be traced back to the seminal works [47], [48]. Current algorithms have been developed for 2D images of limited resolution (width or height < 500 pixels), high-resolution (*i.e.*, 1080p, 4K) [49], [50] and even remote sensing data [51]. According to the supervision strategy, there are five types of SOD models: fully supervised [52], semi-supervised [53], weakly supervised [54], [55], [56], unsupervised [57], [58], [59], and self-supervised [59], [60].

Table 1

Summary of popular SOD datasets. Our SOC is the only one meeting all requirements. According to [76], these datasets can be grouped into three types: early ( $\blacktriangle$ ), popular/modern ( $\blacklozenge$ ), and special ( $\diamond$ ). See § 2.2 for more details.

#	Dataset	Year	Publ.	High-Quality	$\geq 5k$	Non-Salient	Attribute	Category	Bounding Box	Object	Instance
1	MSRA-A, -B [32]	2007	CVPR	✓	✓	-	-	-	✓	✓	-
2	SED1, SED2 [33]	2007	CVPR	✓	-	-	-	-	-	✓	-
3	ASD [82]	2009	CVPR	✓	-	-	-	-	-	✓	-
4	SOD [83]	2010	CVPRW	✓	-	-	-	-	-	✓	-
5	MSRA10K [84]	2011	CVPR	✓	✓	-	-	-	-	✓	-
6	Judd-A [36]	2012	ECCV	✓	-	-	-	-	-	✓	-
7	DUT-O [38]	2013	CVPR	✓	✓	-	-	-	✓	✓	-
8	ECSSD [37]	2013	CVPR	✓	-	-	-	-	-	✓	-
9	PASCAL-S [39]	2014	CVPR	✓	-	-	-	-	-	✓	-
10	HKU-IS [40]	2015	CVPR	✓	-	-	-	-	-	✓	-
11	SOS [63]	2015	CVPR	✓	✓	-	-	-	✓	-	-
12	MSO [63]	2015	CVPR	✓	-	-	-	-	✓	-	-
13	XPIE [85]	2017	CVPR	✓	✓	-	-	-	-	✓	-
14	ILSO [61]	2017	CVPR	-	-	-	-	-	-	-	✓
15	JOT [86]	2017	FCS	✓	✓	✓	-	-	-	✓	-
16	DUTS [41]	2017	CVPR	✓	✓	-	-	-	-	✓	-
17	<b>SOC (OUR)</b>	2021		✓	✓	✓	✓	✓	✓	✓	✓

Recently, several interesting extensions of SOD have also been introduced, such as salient instance detection (SID) [61], [62], salient object subitizing (SOS) [63], [64], [65], and saliency ranking [66], [67]. A taxonomy of the saliency detection task is shown in Fig. 2. Different from previous SOD reviews [68], [69], [70], [71], [72], [73], [74], [75], [76], we mainly focus on 2D salient object detection in a fully supervised manner. We highlight the scope of this study in gray. For other closely related 3D/4D SOD tasks, we refer readers to recent survey and benchmarking works such as RGB-D SOD [77], [78], Event-RGB SOD (ERSOD) <sup>3</sup>, Light Field SOD [79], Co-SOD [80], 360° Video SOD [81], and Video SOD [17].

## 2.2 SOD Datasets

In this section, we briefly discuss existing datasets designed for SOD tasks, focusing in particular on aspects including annotation type, number of salient objects per image, number of images, and image quality. These datasets are listed in Table 1.

Early datasets are either limited in their numbers of images or in their coarse annotations of salient objects. For example, salient objects in the original version of **MSRA-A** [32] and **MSRA-B** [32] are only roughly annotated in the form of bounding boxes. **ASD** [82], **SED1** [33] and **MSRA10K** [35] contain only one salient object in most images, while the **SED2** [33] dataset provides two objects per image but contains only 100 images. In order to improve the quality of datasets, researchers in recent years have started to collect images with multiple objects in relatively complex and cluttered backgrounds. The new datasets include **ECSSD** [37], **DUT-O** [38], **Judd-A** [36], and **PASCAL-S** [39]. These datasets are improved in terms of both annotation quality and number of images, compared to their predecessors. To resolve the shortcomings still present, some datasets (*e.g.*, **HKU-IS** [40], **XPIE** [85], and **DUTS** [41]) provide large amounts of pixel-wise labeled images (Fig. 3.b) with more than one salient object per image. However, they ignore non-salient objects (1<sup>st</sup> row in Fig. 1) and do not offer instance-level annotations (Fig. 3.c). Jiang *et al.* [86] collected roughly 6K *simple background images* (most of them are pure texture images) to cover non-salient scenes. However, their dataset, named **JOT**, falls short in capturing the complexity of real-world scenes. The dataset of **ILSO** [61] contains instance-level salient object annotations but only roughly labeled boundaries, as shown in Fig. 7. Beyond the “standard” SOD datasets, there are



Figure 3. Previous SOD datasets only annotate the images by drawing pixel-accurate silhouettes around salient objects (b). Different from object segmentation datasets [87] (d) where (objects are not necessarily **salient**), our SOC provides *salient instances* (c). We provide a high-quality and large-scale annotated dataset comprised of images that better capture the properties of real-world scenes.

also several other special datasets that introduce new tasks, such as salient object subitizing (*i.e.*, **SOS** [63] and its subset **MSO** [63]).

To sum up, as discussed above, existing datasets mostly focus on images with clear salient objects and simple backgrounds. Considering the aforementioned limitations of existing datasets, a more realistic dataset, containing non-salient objects, textures “in the wild”, and salient objects with attributes, is needed for future investigations in this field. Such a dataset could offer deeper insight into the strengths and weaknesses of SOD models, and help overcome performance saturation. Our **SOC** is unique in that it provides various high-quality annotations, as shown in Table 1.

## 2.3 SOD Models

We have noticed that, from 1998 to the end of Feb. 2021, more than 10,000 papers on saliency detection or related field have been published. In this section, we try our best to summarize those published in top conferences (*e.g.*, NeurIPS, CVPR, ICCV, AAAI) and journals (*e.g.*, TPAMI, TIP, TMM), as well as some high-quality open-access (*i.e.*, arXiv) works. Instead of briefly describing the pipeline of each model, we summarize key components to provide a global view.

As shown in Table 2, a number of different approaches have been designed to tackle SOD using super-pixel, proposal, or edge/boundary annotations under different levels of supervision, such as unsupervised, semi-supervised, and fully supervised. Using common aggregation strategies (*e.g.*, linear, non-linear), these methods mainly focus on pixels, regions, and patches to design more powerful models. Besides, we note that certain priors (*e.g.*, the center-surround prior, local/global contrast prior, fore/background prior, and boundary prior) are frequently used in these methods. Some models also utilize different post-processing steps (*e.g.*, conditional random field, morphology, watershed, and max-flow strategies) to further improve the performance.

3. ERSOD: <https://github.com/jxr326/ERSOD-Net>.

Table 2

Summary of popular SOD models using handcrafted features. **Agg.:** Aggregation strategy, e.g., LN = linear, NL = non-linear, HI = hierarchical, BA = Bayesian, AD = adaptive, LS = least-square solver, EM = energy minimization, and GMRF = Gaussian MRF. **SL.:** Supervision level, e.g., unsupervised (★), semi-supervised (●), weakly supervised (⊂), fully supervised (○), active learning (A). **Sp.:** Whether or not superpixel over-segmentation is used. **Pr.:** Whether or not proposal methods are used. **Ed.:** Whether or not edge cues are used. **Post-Pros.:** Whether post-processing methods (e.g., CRF [88], graph-cut [89], GrabCut [90], Ncut [91]), morphology, max-flow (MF) [92] or only thresholding are used.

#	Model	Publ.	Scholar	Prior.	Uniqueness	Component	Agg.	SL.	Sp.	Pr.	Ed.	Post-Pros	
2010 - 1998	1	Itti [45]	TPAMI	<a href="#">link</a>	center-surround	pixel	Color, Intensity, Orientation	LN	★	-	-	-	
	2	GBVS [93]	NeurIPS	<a href="#">link</a>	-	pixel	Markovian	-	★	-	-	-	
	3	FT [82]	CVPR	<a href="#">link</a>	frequency domain	pixel	Color, Luminance	-	★	-	-	-	
	4	SR [94]	CVPR	<a href="#">link</a>	spectral residual	pixel	Log Spectrum	-	★	-	-	-	
	5	AIM [95]	NeurIPS	<a href="#">link</a>	maximizing information	patch	Shannon's Self-information	-	★	-	-	-	
	6	SUN [96]	JOV	<a href="#">link</a>	self-information	pixel	DoG, ICA-derived features	-	★	-	-	-	
	7	FG [97]	MM	<a href="#">link</a>	local contrast	pixel	Fuzzy Growing	-	★	-	-	-	
	8	AC [98]	ICVS	<a href="#">link</a>	local contrast	multi-patch	Color, Luminance	LN	★	-	-	-	
	9	SEG [99]	ECCV	<a href="#">link</a>	local contrast	pixel	Conditional Probabilistic	-	★	-	-	CRF	
	10	MSSS [100]	ICIP	<a href="#">link</a>	symmetric surround	pixel	Color, Luminance	-	★	-	-	graph-cut	
	11	ICC [101]	ICCV	<a href="#">link</a>	isophote	global structure	curvedness, isocenters, color	LN	★	-	-	graph-cut	
	12	EDS [102]	PR	<a href="#">link</a>	-	pixel	threshold, distance, multi-DoG	-	★	-	✓	-	
	13	RE [103]	ICME	<a href="#">link</a>	local contrast	pixel/patch	Contrast pyramid	-	★	-	-	-	
	14	RSA [104]	MM	<a href="#">link</a>	global contrast	patch	Polar transfer, NN-GPCA [104]	-	★	-	-	-	
	15	RU [105]	TMM	<a href="#">link</a>	rule based	pixel	denoising, geometric	-	★	-	-	-	
	16	CSM [106]	MM	<a href="#">link</a>	frequency&contrast	pixel	Envelope, Skeleton	-	★	-	-	-	
2014 - 2011	17	LSSC [107]	TIP	<a href="#">link</a>	bayesian	pixel/region	convex hull, subspace clustering	NL	★	✓	-	-	
	18	COV [108]	JOV	<a href="#">link</a>	-	pixel/patch	covariance matrices	NL	★	-	-	-	
	19	GR [109]	SPL	<a href="#">link</a>	contrast, center, smooth	-	convex hull, continuous pair	NL	★	✓	-	-	
	20	MSS [110]	SPL	<a href="#">link</a>	local, integrity, center	-	various gaussian, convex hull	NL	★	✓	-	-	
	21	LSMD [111]	AAAI	<a href="#">link</a>	texture, edge, color	pixel/region	hierarchical clustering, gaussian	-	★	✓	✓	threshold	
	22	BSF [112]	ICIP	<a href="#">link</a>	boundary-based	region	convex hull, soft-segmentation	-	★	✓	-	-	
	23	HC [84]	CVPR	<a href="#">link</a>	global contrast	region	Histogram-based Contrast	-	★	-	-	graph-cut	
	24	RC [84]	CVPR	<a href="#">link</a>	global contrast	region	Region-based Contrast	-	★	-	-	graph-cut	
	25	CA [84]	CVPR	<a href="#">link</a>	context-aware	patch	Four principles	-	★	-	-	-	
	26	MR [38]	CVPR	<a href="#">link</a>	fore/back-ground	pixel/region	graph-based manifold ranking	-	★	✓	-	-	
	27	SF [113]	CVPR	<a href="#">link</a>	element contrast	region	uniqueness, spatial	NL	★	-	-	-	
	28	HS [37]	CVPR	<a href="#">link</a>	global contrast	hi-region	Region-scale, Location heuristic	HI	★	-	-	-	
	29	DRFI [114]	CVPR	<a href="#">link</a>	background descriptor	region	region vector, multi-level	LN	○	✓	-	-	
	30	RBD [115]	CVPR	<a href="#">link</a>	background weighted	region	background connectivity	LS	★	✓	-	-	
	31	LR [116]	CVPR	<a href="#">link</a>	location, semantic, color	pixel/region	Low rank matrix	NL	○	✓	-	threshold	
	32	PCA [117]	CVPR	<a href="#">link</a>	center-bias priors	patch	color, pattern, gaussian	NL	★	✓	-	-	
	33	HDCT [118]	CVPR	<a href="#">link</a>	high-dimensional color	pixel	Trimap, color transform	LN	★	✓	-	-	
	34	CRFM [119]	CVPR	<a href="#">link</a>	aggregation	pixel	GIST descriptor	NL	○	-	-	CRF	
	35	STD [120]	CVPR	<a href="#">link</a>	statistical textural	region	Graph, sparse texture	-	★	-	-	GrabCut	
	36	PDE [121]	CVPR	<a href="#">link</a>	representative elements	region	color, background, center	-	○	✓	-	-	
	37	SUB [122]	CVPR	<a href="#">link</a>	Submodular	region	color, spatial, center	-	○	✓	-	threshold	
	38	PISA [123]	CVPR	<a href="#">link</a>	spatial	pixel/region	color, structure, orientation	NL	★	-	-	✓	
	39	DSR [124]	ICCV	<a href="#">link</a>	reconstruction errors	multi-region	background, obj./centerGaussian	BA	★	✓	-	-	
	40	MC [125]	ICCV	<a href="#">link</a>	markov random walks	region	Markov Chain	-	★	✓	-	-	
	41	GC [126]	ICCV	<a href="#">link</a>	global cue	region	GMM, appearance, spatial	AD	★	-	-	-	
	42	SVO [127]	ICCV	<a href="#">link</a>	center-surround	patch/region	Graph, Obj.	EM	★	✓	-	-	
	43	CSD [128]	ICCV	<a href="#">link</a>	center-surround	multi-patch	color, orientation, intensity	LN	★	-	-	-	
	44	UFO [129]	ICCV	<a href="#">link</a>	focus, objectness	pixel/region	Uniqueness, Focusness, Obj.	NL	★	✓	✓	threshold	
	45	CHM [130]	ICCV	<a href="#">link</a>	center-surround, local	mRegion/patch	SVM, hyperedge	LN	●	✓	✓	threshold	
	46	CIO [131]	ICCV	<a href="#">link</a>	objectness	Region	Graph, frequency, Obj.	GMRF	★	✓	-	-	
47	CC [132]	ICCV	<a href="#">link</a>	convexity context	mRegion	concavity, bounding box	-	★	✓	-	graph-cut		
48	GS [133]	ECCV	<a href="#">link</a>	boundary, connectivity	patch/region	Geodesic distance transform	-	★	✓	-	✓		
49	CB [134]	BMVC	<a href="#">link</a>	context, shape, center	mRegion	Iterative energy minimization	LN	★	✓	✓	-		
50	SLMR [135]	BMVC	<a href="#">link</a>	low-rank matrix	Region	sparse noise	-	★	✓	-	-		
2018 - 2015	51	SMD [136]	TPAMI	<a href="#">link</a>	texture, edge, color	pixel/region	hierarchical clustering, gaussian	-	★	✓	✓	threshold	
	52	RS [137]	TPAMI	<a href="#">link</a>	fore/back-ground	region	manifold ranking, grouping cue	-	★	✓	-	-	
	53	BFS [138]	NC	<a href="#">link</a>	fore/back-ground seed	region	Gaussian falloff, threshold	NL	★	✓	-	-	
	54	GLC [139]	PR	<a href="#">link</a>	global/local contrast	region	HOG, LBP, codebook, graph-cut	LN	★	✓	-	-	
	55	DSP [140]	PR	<a href="#">link</a>	propagation	region	sink points, chi-square distance	NL	★	✓	✓	-	
	56	LPS [141]	TIP	<a href="#">link</a>	label propagation-base	pixel/region	three-cue-center, affinity matrix	NL	★	✓	-	-	
	57	MAPM [142]	TIP	<a href="#">link</a>	background	region	Markov absorption probability	-	★	✓	-	-	
	58	MIL [143]	TIP	<a href="#">link</a>	instance	region	multi-instance learning, SVM	-	●	✓	✓	-	
	59	RCRR [144]	TIP	<a href="#">link</a>	reversion correction	pixel/region	regular-random walks ranking	-	★	✓	-	-	
	60	FCB [145]	TIP	<a href="#">link</a>	fore/back-ground, center	region	color difference, color volume	NL	★	✓	-	-	
	61	NCS [146]	TIP	<a href="#">link</a>	center bias	pixel/region	Ncut, merging scheme	EM	★	✓	-	✓	
	62	MDC [147]	TIP	<a href="#">link</a>	direction contrast	pixel	OTSU, morphological filter	NL	★	-	-	watershed	
	63	HCCH [148]	TIP	<a href="#">link</a>	closure completeness & reliability	object	hierarchical segmentation	NL	★	-	✓	-	
	64	JLSE [149]	TIP	<a href="#">link</a>	exemplar-aided	region	joint latent space embedding	-	○	✓	-	-	
	65	IFC [150]	TMM	<a href="#">link</a>	boundary homogeneity	pixel/region	linear feedback control system	-	○	✓	-	-	
	66	NIO [151]	TNNLS	<a href="#">link</a>	smoothness, boundary	region	graph, iterative optimization	BA	●	✓	-	-	
	67	MBS [152]	ICCV	<a href="#">link</a>	barrier distance	pixel	backgroundness cue	-	★	✓	-	morphology	
	68	GP [153]	ICCV	<a href="#">link</a>	diffusion based	region/pixel	diffusion/laplacian matrix	-	★	✓	-	-	
	69	BSCA [154]	CVPR	<a href="#">link</a>	color/space contrast	region/pixel	cellular automata, bayesian	-	★	✓	-	OTSU [155]	
	70	BL [156]	CVPR	<a href="#">link</a>	image prior	mRegion	SVM, MKB [157], LBP	LN	○	✓	-	-	
	71	MST [158]	CVPR	<a href="#">link</a>	geometry information	pixel	minimum spanning tree	-	★	✓	-	morphology	
	72	RRWR [159]	CVPR	<a href="#">link</a>	error-boundary removal	pixel/region	regular-random walks ranking	-	★	✓	-	-	
	73	LLL [160]	CVPR	<a href="#">link</a>	propagation, boundary	region	convex hull, teach-to-learn	-	★	✓	-	-	
	74	WSC [161]	CVPR	<a href="#">link</a>	weighted sparse coding	region	color histogram, dictionary	NL	★	✓	-	-	
	75	PM [162]	ECCV	<a href="#">link</a>	propagation	region	extended random walk	LN	★	✓	-	-	
2021 - 2019	76	TSG [163]	TCSVT	<a href="#">link</a>	regionally spatial consistency	region	Sparse Representation, graph	LN	★	✓	-	-	MF
	77	LFCS [53]	TCSVT	<a href="#">link</a>	smoothness, boundary	region	Discrete Linear Control System	LN	●	✓	-	-	-
	78	AIGC [164]	TCSVT	<a href="#">link</a>	contrast, object	region	irregular graph	-	●	✓	-	-	-
	79	FTOE [165]	TMM	<a href="#">link</a>	contrast, center, distribute	pixel/region	fuzzy theory, object enhancement	LN	★	✓	✓	-	-
	80	MSGC [166]	TMM	<a href="#">link</a>	fore/back-ground seed	region	multi-scale, global cue	NL	★	✓	-	-	
	81	SIA [167]	TMM	<a href="#">link</a>	boundary, dhs [168]	-	Cellular Automata	BA	★	✓	-	-	
	82	KSR [169]	TIP	<a href="#">link</a>	trained on [32]	region	R-CNN, Rank-SVM, subspace	-	A	✓	-	-	
	83	MSR [170]	TIP	<a href="#">link</a>	boundary connectivity	region	MBD [171]	-	★	✓	-	-	OTSU
84	LRR [172]	TIP	<a href="#">link</a>	background	pixel/region	Cellular Automata [154], FCN32	Metric	★	✓	-	-	-	

Table 3

Summary of popular deep learning based SOD models. See Table 2 for more detailed descriptions. MB = MSRA-B dataset [32]. M10K = MSRA-10K [35] dataset. P-VOC2010 = PASCAL VOC 2010 semantic segmentation dataset [173]. CRF = Conditional random fields. **Clicking the scholar will link to the specific author's google scholar.**

	#	Model	Publ.	Scholar	#Training	Training Dataset	Backbone	SL	Sp.	Pr.	Ed.	CRF
2015	1	SupCNN [174]	IJCV	<a href="#">link</a>	800	ECSSD [37]	-	o	✓	-	-	-
	2	LEGS [175]	CVPR	<a href="#">link</a>	340+3,000	PASCAL-S [39]+MB [32]	-	o	-	✓	-	-
	3	MDF [40]	CVPR	<a href="#">link</a>	2,500	MB [32]	-	o	✓	-	✓	-
	4	MC [176]	CVPR	<a href="#">link</a>	8,000	M10K [35]	GoogLeNet [177]	o	✓	-	-	-
2016	5	DSL [178]	TCSVT	<a href="#">link</a>	(5,168+10,000)*80%	DUT-O [38]+M10K [35]	LeNet [179]/VGGNet16	o	✓	-	-	-
	6	DISC [180]	TNNLS	<a href="#">link</a>	9,000	M10K [35]	-	o	✓	-	-	-
	7	DS [181]	TIP	<a href="#">link</a>	10,000	M10K [35]	VGGNet [182]	o	✓	-	✓	✓
	8	SSD [183]	ECCV	<a href="#">link</a>	2,500	MB [32]	AlexNet [184]	o	✓	✓	-	-
	9	CRPSD [185]	ECCV	<a href="#">link</a>	10,000	M10K [35]	VGGNet	o	✓	-	-	-
	10	RFCN [186]	ECCV	<a href="#">link</a>	10,103+10,000	P-VOC2010 [173]+M10K [35]	VGGNet	o	✓	-	✓	-
	11	MAP [187]	CVPR	<a href="#">link</a>	~5,500	SOS [63]	VGGNet	o	-	-	-	-
	12	SU [188]	CVPR	<a href="#">link</a>	15,000+10,000	SALI [189]+M10K [35]	VGGNet	o	-	-	-	✓
	13	RACD [190]	CVPR	<a href="#">link</a>	10,565	DUT-O [38]+NJU [191]+NLP [192]	VGGNet	o	-	-	-	-
	14	ELD [193]	CVPR	<a href="#">link</a>	9,000	M10K [35]	VGGNet	o	✓	-	-	-
	15	DHS [168]	CVPR	<a href="#">link</a>	3,500+6,000	DUT-O [38]+M10K [35]	VGGNet	o	-	-	-	-
16	DCL [194]	CVPR	<a href="#">link</a>	2,500	MB [32]	VGGNet	o	✓	-	-	✓	
2017	17	DLS [195]	CVPR	<a href="#">link</a>	10,000	M10K [35]	VGGNet	o	✓	-	-	-
	18	MSRNet [61]	CVPR	<a href="#">link</a>	(500+)+2,500+2,500	(ILSO [61]+)MB [32]+HKU-IS [40]	VGGNet	o	-	✓	✓	✓
	19	SRM [196]	CVPR	<a href="#">link</a>	10,553	DUTS [41]	ResNet50 [197]	o	-	-	-	-
	20	NLDF [198]	CVPR	<a href="#">link</a>	2,500	MB [32]	VGGNet	o	-	-	✓	✓
	21	WSS [41]	CVPR	<a href="#">link</a>	456K	ImageNet [199]	VGGNet	o	✓	-	-	✓
	22	DSS [200]	CVPR	<a href="#">link</a>	2,500	HKU-IS [40]+MB [32]	VGGNet	o	-	-	✓	✓
	23	FSN [201]	ICCV	<a href="#">link</a>	10,000	M10K [35]	VGGNet	o	-	-	-	-
	24	SVF [202]	ICCV	<a href="#">link</a>	10,000	M10K [35]	VGGNet	o	✓	-	-	-
	25	UCF [203]	ICCV	<a href="#">link</a>	10,000	M10K [35]	VGGNet	o	-	-	-	-
	26	AMU [204]	ICCV	<a href="#">link</a>	10,000	M10K [35]	VGGNet	o	-	-	✓	-
2018	27	EAR [205]	TCYB	<a href="#">link</a>	2,500+2,500	HKU-IS [40]+MB [32]	VGGNet16	o	-	-	-	-
	28	Refinet [206]	TMM	<a href="#">link</a>	3,000	MB [32]	VGGNet16	o	✓	-	✓	✓
	29	LICNN [207]	AAAI	<a href="#">link</a>	456K	ImageNet [199]	VGGNet	o	-	-	-	-
	30	ASMO [54]	AAAI	<a href="#">link</a>	82,783+2,500+2,500	MsCO [87]+HKU-IS [40]+MB [32]	ResNet101	o	-	-	-	✓
	31	RADF [208]	AAAI	<a href="#">link</a>	10,000	M10K [35]	VGGNet	o	-	-	-	✓
	32	R3Net [209]	IJCAI	<a href="#">link</a>	10,000	M10K [35]	ResNeXt [210]	o	-	-	-	✓
	33	C2SNet [211]	ECCV	<a href="#">link</a>	20,000+10,000	Web [211]+M10K [35]	VGGNet	o	✓	✓	-	-
	34	RAS [212]	ECCV	<a href="#">link</a>	2,500	MB [32]	VGGNet	o	-	-	-	-
	35	LPSNet [213]	CVPR	<a href="#">link</a>	10,553	DUTS [41]	VGGNet16	o	-	-	-	-
	36	RSOD [214]	CVPR	<a href="#">link</a>	425	PASCAL-S [39]	ResNet101	o	-	✓	-	-
	37	DUS [58]	CVPR	<a href="#">link</a>	2,500	MB [32]	ResNet101	o	-	-	-	-
	38	ASNet [215]	CVPR	<a href="#">link</a>	15,000+10,000+5,168	SALI [189]+M10K [35]+DUT-O [38]	VGGNet	o	-	-	-	-
	39	BMPM [216]	CVPR	<a href="#">link</a>	10,553	DUTS [41]	VGGNet	o	-	-	-	-
40	DGRL [217]	CVPR	<a href="#">link</a>	10,553	DUTS [41]	ResNet50	o	-	-	-	-	
41	PiCA [218]	CVPR	<a href="#">link</a>	10,553	DUTS [41]	VGGNet16/ResNet50	o	-	-	-	✓	
42	PAGRN [219]	CVPR	<a href="#">link</a>	10,553	DUTS [41]	VGGNet19	o	-	-	-	-	
2019	43	SE2Net [220]	arXiv	<a href="#">link</a>	10,553	DUTS [41]	VGGNet/ResNeXt101	o	-	-	-	-
	44	DRMC [221]	arXiv	<a href="#">link</a>	10,533	DUTS [41]	VGGNet/ResNet101	o	-	-	-	✓
	45	RDSNet [222]	arXiv	<a href="#">link</a>	10,000+10,553	M10K [35]+DUTS [41]	VGGNet/ResNet-152	o	-	-	-	✓
	46	AADF [223]	TCSVT	<a href="#">link</a>	10,553	DUTS [41]	DenseNet161 [224]	o	-	-	-	-
	47	CCAL [225]	TMM	<a href="#">link</a>	9,000	M10K [35]	VGGNet	o	-	-	-	-
	48	DeepUSPS [59]	NeurIPS	<a href="#">link</a>	2,500	MB [32]	DRN-network [226]	o	-	-	-	-
	49	FBG [227]	TIP	<a href="#">link</a>	2,500	MB [32]	VGGNet16	o	-	-	✓	-
	50	SPA [228]	TIP	<a href="#">link</a>	4,000	HKU-IS [40]	-	o	✓	-	-	✓
	51	ConnNet [229]	TIP	<a href="#">link</a>	2,500+2,500	MB [32]+HKU-IS [40]	ResNet50	o	-	-	-	-
	52	LFRWS [230]	TIP	<a href="#">link</a>	10,000	M10K [35]	VGGNet16	o	-	-	✓	-
	53	RSR [66]	TPAMI	<a href="#">link</a>	425	Extended of PASCAL-S [39]	ResNet101	o	-	-	-	-
	54	SSNet [231]	TPAMI	<a href="#">link</a>	10,000	M10K [35]	VGGNet16	o	✓	-	-	-
	55	LVNet [232]	TGRS	<a href="#">link</a>	600	ORSSD [232]	-	o	-	-	-	-
	56	DeepSide [233]	NC	<a href="#">link</a>	2,500+10,553	MB [32]+DUTS [41]	VGGNet16	o	✓	-	-	-
	57	SuperVAE [234]	AAAI	<a href="#">link</a>	-	-	VGGNet19	o	✓	-	-	-
	58	DEF [235]	AAAI	<a href="#">link</a>	10,553	DUTS [41]	ResNet101	o	-	-	-	-
	59	CapSal [55]	CVPR	<a href="#">link</a>	82,783+5,265	MsCO [87]+COCO-CapSal [55]	ResNet101	o	-	-	-	-
	60	MWS [236]	CVPR	<a href="#">link</a>	300,000+10,553	ImageNet [199]+DUTS [41]	ResNet101	o	✓	-	-	✓
	61	MLMS [237]	CVPR	<a href="#">link</a>	10,553	DUTS [41]	VGGNet16	o	-	-	-	✓
	62	ICNet [238]	CVPR	<a href="#">link</a>	10,000	M10K [35]	VGGNet16/ResNet50	o	-	-	-	✓
63	AFNet [239]	CVPR	<a href="#">link</a>	10,533	DUTS [41]	VGGNet16	o	-	-	✓	-	
64	PFANet [240]	CVPR	<a href="#">link</a>	10,553	DUTS [41]	VGGNet16	o	-	-	✓	-	
65	PAGE [241]	CVPR	<a href="#">link</a>	10,000	M10K [35]	VGGNet16	o	-	-	✓	✓	
66	CPD [242]	CVPR	<a href="#">link</a>	10,533	DUTS [41]	VGGNet/ResNet50	o	-	-	-	-	
67	PoolNet [243]	CVPR	<a href="#">link</a>	10,533	DUTS [41]	VGGNet/ResNet	o	-	-	✓	-	
68	BASNet [244]	CVPR	<a href="#">link</a>	10,553	DUTS [41]	ResNet34/Xavier [245]	o	-	-	✓	-	
69	JDF [246]	ICCV	<a href="#">link</a>	2,500	MB [32]	VGGNet16	o	-	-	✓	-	
70	DPOR [247]	ICCV	<a href="#">link</a>	10,533	DUTS [41]	VGGNet16	o	-	-	-	-	
71	JLNet [248]	ICCV	<a href="#">link</a>	10,582+10,533	P-VOC2010 [173]+DUTS [41]	DenseNet169	o	-	-	-	✓	
72	GLFN [50]	ICCV	<a href="#">link</a>	1,600+10,533	HRSOD [50]+DUTS [41]	VGGNet	o	-	-	-	✓	
73	SIBA [249]	ICCV	<a href="#">link</a>	10,533	DUTS [41]	ResNet50	o	-	-	✓	-	
74	SCRNet [44]	ICCV	<a href="#">link</a>	10,533	DUTS [41]	ResNet50	o	-	-	✓	-	
75	EGNet [250]	ICCV	<a href="#">link</a>	10,533	DUTS [41]	VGGNet/ResNet	o	-	-	✓	-	
2020	76	HUAN [251]	TIP	<a href="#">link</a>	10,553	DUTS [41]	VGGNet/ResNet/ResNetXt	o	-	-	-	✓
	77	ALM [252]	TIP	<a href="#">link</a>	10,000+4,447	M10K [35]+HKU-IS [40]	DenseNet	o	✓	-	-	-
	78	HFFNet [253]	TIP	<a href="#">link</a>	10,553	DUTS [41]	VGGNet16	o	-	-	✓	-
	79	DFI [254]	TIP	<a href="#">link</a>	10,553	DUTS [41]	ResNet50	o	-	-	✓	-
	80	R2Net [255]	TIP	<a href="#">link</a>	10,553	DUTS [41]	VGGNet16	o	-	-	-	-
	81	MRNet [256]	TIP	<a href="#">link</a>	10,553	DUTS [41]	ResNet50	o	-	-	-	-
	82	CIG [257]	TIP	<a href="#">link</a>	10,000	M10K [35]	VGGNet16	o	-	-	✓	-
	83	RASNet [258]	TIP	<a href="#">link</a>	2,500	MB [32]	VGGNet16	o	-	-	-	-
	84	ASNet [259]	TPAMI	<a href="#">link</a>	15,000+10,000+5,168	SALI [189]+M10K [35]+DUT-O [38]	VGGNet	o	-	-	-	-
	85	DNNet [260]	TCYB	<a href="#">link</a>	2,500+2,500	MB [32]+HKU-IS [40]	-	o	-	-	-	-
	86	CAANet [261]	TCYB	<a href="#">link</a>	10,553	DUTS [41]	VGGNet16	o	-	-	-	-
	87	ROSA [262]	TCYB	<a href="#">link</a>	2,500+5,168+2,500	HKU-IS [40]+DUT-O [38]+MB [32]	VGGNet16	o	-	-	-	-
	88	DSRNet [264]	TCSVT	<a href="#">link</a>	10,553	DUTS [41]	FCN [263]	o	✓	-	-	-
	89	EGNL [265]	TCSVT	<a href="#">link</a>	2,500	MB [32]	VGGNet16	o	-	-	✓	-
	90	SACNet [266]	TCSVT	<a href="#">link</a>	10,553	DUTS [41]	DenseNet	o	-	-	-	-
	91	FLGC [267]	TMM	<a href="#">link</a>	10,553	DUTS [41]	VGGNet16	o	-	-	-	-
	92	TSNet [268]	TMM	<a href="#">link</a>	4,000	MD4K [268]	ResNet50/VGGNet16	o	-	-	-	-

Table 4  
Summary of popular deep learning based SOD models. See Tables 2 & 3 for more detailed descriptions.

	#	Model	Publ.	Scholar	#Training	Training Dataset	Backbone	SL.	Sp.	Pr.	Ed.	CRF	
2020	93	SUCA [269]	TMM	<a href="#">link</a>	10,553	DUTS [41]	ResNet50	o	-	-	-	-	
	94	MJR [270]	TMM	<a href="#">link</a>	2,500+5,000	MB [32]+DUTS [41]	VGGNet16	o	✓	✓	-	✓	
	95	CAGVgg [271]	PR	<a href="#">link</a>	10,553	DUTS [41]	VGGNet/ResNet/NASNet [272]	o	-	-	-	-	
	96	U2Net [273]	PR	<a href="#">link</a>	10,553	DUTS [41]	UNet	o	-	-	-	-	
	97	SalGAN [274]	TIJ	<a href="#">link</a>	10,000	M10K [35]	VGGNet16	o	-	-	-	-	
	98	ADA [275]	AAAI	<a href="#">link</a>	2,500+780	MB [32]+NIR [275]	VGGNet16	o	-	-	-	-	
	99	PFPNet [276]	AAAI	<a href="#">link</a>	10,553	DUTS [41]	ResNet101	o	-	-	-	-	
	100	GCPANet [277]	AAAI	<a href="#">link</a>	10,553	DUTS [41]	ResNet50	o	-	-	-	-	
	101	F3Net [278]	AAAI	<a href="#">link</a>	10,553	DUTS [41]	ResNet50	o	-	-	✓	-	
	102	LDF [279]	CVPR	<a href="#">link</a>	10,553	DUTS [41]	ResNet50	o	-	-	✓	-	
	103	ITSD [280]	CVPR	<a href="#">link</a>	10,553	DUTS [41]	VGGNet16/ResNet50	o	-	-	✓	-	
	104	SANet [56]	CVPR	<a href="#">link</a>	10,553	DUTS [41]	VGGNet16	o	-	-	✓	✓	
	105	MINet [281]	CVPR	<a href="#">link</a>	10,553	DUTS [41]	VGGNet16/ResNet50	o	-	-	-	-	
	106	ABPNet [282]	ECCV	<a href="#">link</a>	10,553	DUTS [41]	VGGNet16	o	-	-	✓	-	
	107	CSNet [283]	ECCV	<a href="#">link</a>	10,553	DUTS [41]	-	o	-	-	-	-	
	108	GateNet [284]	ECCV	<a href="#">link</a>	10,553	DUTS [41]	VGGNet16	o	-	-	-	✓	
	2021	109	DNA [285]	TCYB	<a href="#">link</a>	10,553	DUTS [41]	VGGNet16/ResNet50	o	-	-	-	-
		110	DAFNet [51]	TIP	<a href="#">link</a>	1,400	EORSSD [51]	VGGNet16	o	-	-	✓	-
111		HGA [286]	TIP	<a href="#">link</a>	10,553	DUTS [41]	VGGNet16	o	-	-	✓	-	
112		HIRN [287]	TIP	<a href="#">link</a>	10,553	DUTS [41]	VGGNet16	o	-	-	✓	-	
113		SCWS [288]	AAAI	<a href="#">link</a>	10,553	SDUTS [56]	ResNet50	o	-	-	✓	-	
114		PFS [289]	AAAI	<a href="#">link</a>	10,553	DUTS [41]	ResNet50	o	-	-	✓	-	
115		KRNet [290]	AAAI	<a href="#">link</a>	10,553	DUTS [41]	ResNet50	o	-	-	✓	-	
116		BAS [31]	arXiv	<a href="#">link</a>	10,553	DUTS [41]	ResNet34/Xavier	o	-	-	✓	-	
117		ICON [52]	arXiv	<a href="#">link</a>	10,553	DUTS [41]	ResNet50	o	-	-	-	-	

More recently, many deep learning SOD models based on different network architectures, such as multi-layer perceptrons, fully convolutional networks (FCNs), hybrid networks and capsules, have been proposed and achieve higher performance than traditional methods. According to the learning paradigm, most deep SOD models can be roughly split into two types: single-task learning and multi-task learning methods. We summarize the training data, backbones, and other components in Tables 3 and 4.

We mainly focus on macro-level statistics rather than micro-level descriptions. We kindly refer readers to the recent architecture review [76]. We hope this comprehensive review can serve as guidance<sup>4</sup> for future researchers in this fast-growing field.

## 2.4 Dataset-Enhancement Strategies for Deep Models

Existing deep SOD models focus on designing effective decoders [44], [51], [260], [261], [264], [278], [285] to aggregate features from different levels of the backbone network [197], [210], [291]. We argue that, as they employ a mapping function from the input training image set to the output training ground-truth set, deep models should also focus on dataset-enhancement strategies to improve model generalization ability. Three different strategies have been widely studied, including label smoothing [292], image augmentation [293], [294], and self-supervised learning [295].

Instead of training directly with one-hot supervision, “label smoothing” techniques learn from smoothed supervision, and can thus relax the supervision signals using the generated smoothing labels [292] or disturbed labels [296]. Miyato *et al.* [297] applied local perturbations to data points to increase the smoothness of the model distribution. Thulasidasan *et al.* [298] discovered that mix-up training [294] with label smoothing can significantly improve model calibration. To obtain a more robust and generative model, Xie *et al.* [296] randomly replaced a portion of labels with incorrect values in each iteration. In addition, Wager *et al.* [299] demonstrated that corrupting training examples with noise from known distributions within the exponential family can inject appropriate generative assumptions into discriminative models, thus reducing generalization errors. Peterso *et al.* presented a soft-label dataset (CIFAR10H [300]) aiming at reflecting human

perceptual uncertainty by providing label distributions across categories instead of hard one-hot labels.

Image augmentation [293] is an effective technique for extending the diversity of a training dataset, thus improving model generalization ability. Existing data augmentation techniques can be roughly divided into two categories: 1) human-designed policies, *e.g.*, rotation or scale transformation, and 2) learned policies [301], [302]. For the former, a predefined data augmentation policy is applied to the dataset. Beside the widely used rotation and scale transformations, other extensively studied methods in this category are erasing techniques [303], [304], which achieve data augmentation by randomly erasing part of the image patch. Further, mix-up methods [305], [306] utilize the mix-up data augmentation strategy to generate new samples from an existing training dataset to mitigate the uncertainty in prediction. For the latter [301], the network learns an image-conditioned data augmentation policy, which is usually parameterized by a deep neural network. In this way, the input image is fed to the data augmentation network to generate augmented samples with hyperparameters that control the degree of data augmentation.

Self-supervised learning [295], [307], also termed as consistency learning, defines an annotation-free pretext task to provide a surrogate supervision signal for feature learning. Conventionally, self-supervised learning is used for unsupervised representation learning to learn the feature embedding of the image or video. Recently, works have defined self-supervised learning as an auxiliary task, and used it within a weakly supervised [288] or semi-supervised learning framework [308]. Several recent and representative arts can be found in [309], [310], [311].

As far as we know, no existing salient object detection works have focused on exploring the dataset bias issue with dataset-enhancement strategies. In this paper, we claim that efforts on developing dataset-improvement strategies can also yield significant performance gains. Further, these solutions are general and can be easily applied to existing saliency detection networks.

## 3 SOC DATASET

In this section, we present details of our new challenging *SOC* dataset designed to reflect real-world scenes. Sample images from *SOC* are shown in Fig. 1, while statistics regarding the

4. Research group: <https://github.com/DengPingFan/Saliency-Authors>.

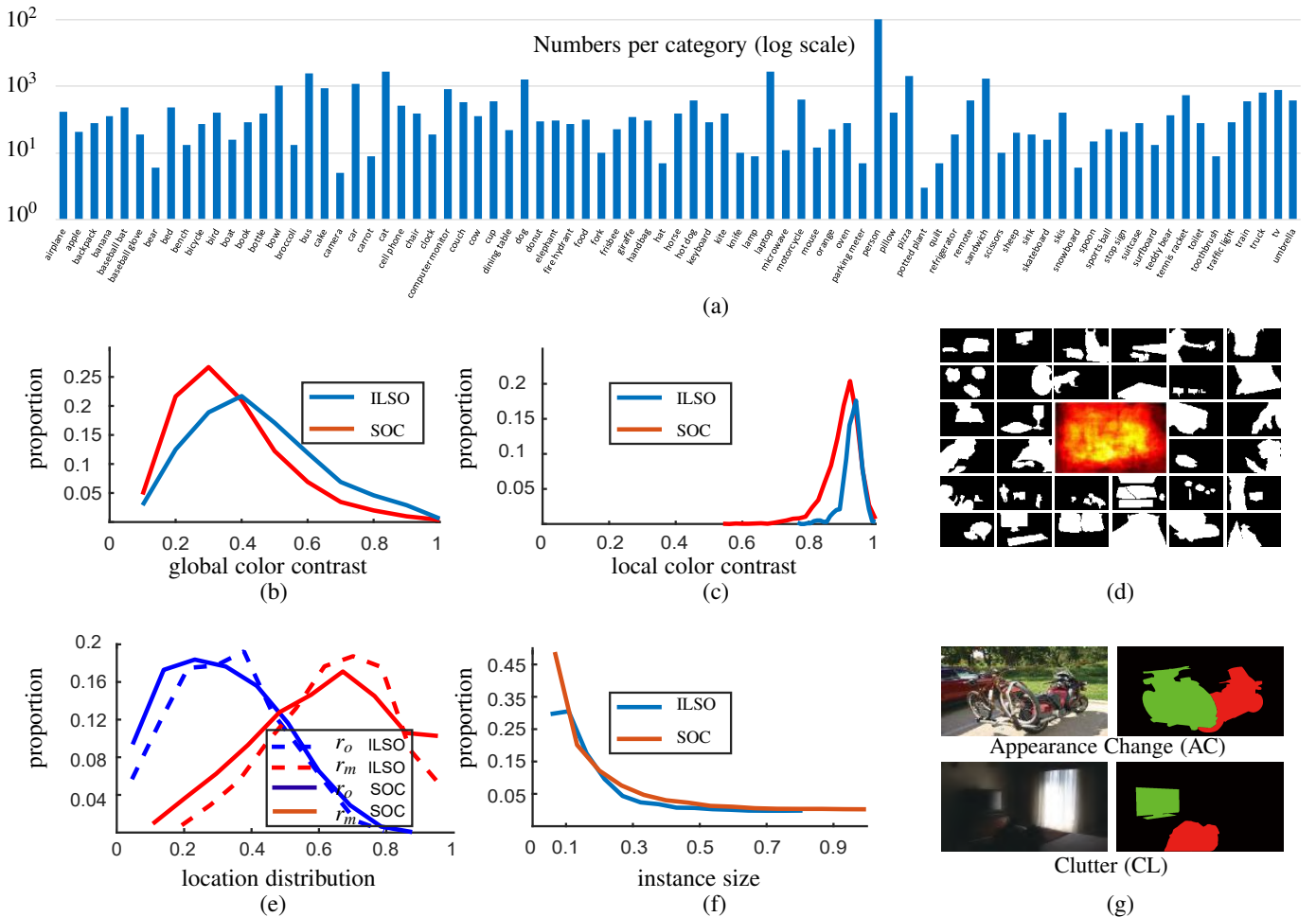


Figure 4. (a) Number of annotated instances per category in our SOC dataset. (b, c) Global and local color contrast statistics, respectively. (d) A set of saliency maps from our dataset and their overlay map. (e) Location distribution of the salient objects in SOC. (f) Distribution of instance sizes in the SOC and ILSO [61] datasets. (g) Visual examples of attributes. Best view on screen and zoomed-in for details.

categories and attributes are shown in Fig. 4 (a) and Fig. 6, respectively. Based on the strengths and weaknesses of existing datasets, we identify seven crucial requirements that a comprehensive and balanced dataset should fulfill.

**1) Presence of Non-Salient Objects.** Most existing SOD datasets assume that an image should contain at least one salient object and thus discard images without salient objects [86]. However, this assumption is only true under ideal settings, which leads to *data selection bias*. In realistic settings, images do not always contain salient objects. For example, some images of amorphous backgrounds, such as sky, grass or textures, contain no salient objects at all [312]. The non-salient objects or background “stuff” may occupy the entire scene, and hence heavily constrain the possible locations of a salient object. Xia *et al.* [85] proposed

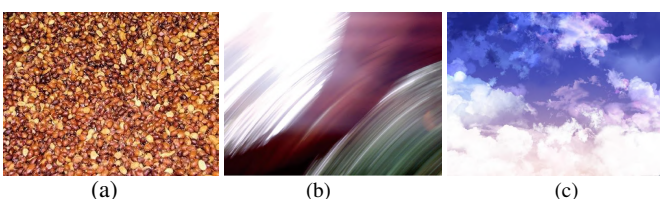


Figure 5. Examples of non-salient objects in our dataset. a) Crowded scene, b) motion blur, and c) background with non-interesting regions.

a state-of-the-art SOD model that determines what is or is not a salient object, indicating that non-salient objects are crucial for reasoning salient objects. This suggests that non-salient objects deserve equal attention in SOD. Incorporating images containing non-salient objects makes a dataset more realistic, and hence more challenging. We define “*non-salient objects*” as images without salient objects or images with “stuff” categories. As suggested in [85], [312], the “stuff” categories include (a) densely distributed similar objects, (b) fuzzy shapes, and (c) regions without semantics, as illustrated in Fig. 5 (a)-(c), respectively.

To avoid data selection bias, we selected images randomly and automatically, as suggested by Torralba and Efros [43]. Based on the characteristics of non-salient objects, we randomly collected 783 texture images from the DTD [313] dataset. To enrich the diversity, 2,217 images including aurora, sky, crowds, store and many other kinds of realistic scenes were gathered from the Internet and other datasets [34], [39], [86], [87].

**2) Number and Categories of Images.** Providing a large number of images is essential for capturing the diversity and abundance of real-world scenes. Moreover, with large amounts of data, SOD models can avoid overfitting and enhance generalization. To this end, we first randomly gathered 3,000 images from the MSCOCO dataset [87], which contains ‘everyday scenes of common objects in their **natural** context.’ Then, more than 80 object

Table 5

List of salient object image attributes and their corresponding descriptions. These attributes are derived by studying the characteristics of existing datasets. Some visual examples can be found in Fig. 1 and Fig. 4 (g). For more examples, please refer to the supplementary materials.

Attribute	Description
AC ( <i>Appearance Change</i> )	Obvious illumination change in the object region.
BO ( <i>Big Object</i> )	The ratio between the object area and the image area is larger than 0.5.
CL ( <i>Clutter</i> )	Foreground and background regions around the object have similar colors. We labeled images with a global color contrast value larger than 0.2 and local color contrast value smaller than 0.9 as cluttered images (§ 3).
HO ( <i>Heterogeneous Objects</i> )	Objects composed of visually distinctive/dissimilar parts.
MB ( <i>Motion Blur</i> )	Objects have fuzzy boundaries due to camera shaking or motion.
OC ( <i>Occlusion</i> )	Objects are partially or fully occluded.
OV ( <i>Out-of-View</i> )	Part of the object is clipped by the image boundaries.
SC ( <i>Shape Complexity</i> )	Objects have complex boundaries, such as thin parts ( <i>e.g.</i> , the foot of animal) and holes.
SO ( <i>Small Object</i> )	The ratio between the object area and the image area is smaller than 0.1.

categories (see supplementary materials) were annotated. Note that we separated the process of data selection and labeling to avoid data selection bias, as discussed in [43]. Please refer to the subsection “7) High-Quality Salient Object Labeling” for details on this. Fig. 4 (a) shows the number of salient objects in each category. As can be seen, the “person” category accounts for a large proportion of the data, which is reasonable as people usually appear in daily scenes along with other objects. We divided our dataset (3k non-salient images and 3k salient images) into training, validation and test sets in the ratio of 6:2:2.

**3) Global vs. Local Color Contrast of Salient Objects.** As described in [39], the term “salient” is related to the global/local contrast of the foreground and background. It is essential to confirm whether the salient objects are easy to detect. For each object, we compute separate RGB color histograms for the foreground and background. Then,  $\chi^2$  distance is utilized to measure the distance between the two histograms. The global and local color contrast distributions are shown in Fig. 4 (b) and (c), respectively. Compared to ILSO, the SOC dataset has a higher proportion of objects with low global and local color contrast.

**4) Locations.** *Center bias* has been identified as one of the most significant and challenging biases pertaining to saliency detection datasets [39], [69], [314]. Fig. 4 (d) illustrates a set of images and their overlay map (*i.e.*, average mask map). As can be seen, although salient objects are located at different positions, the overlay map shows that somehow these images are still center biased. Unfortunately, previous benchmarks have often adopted this incorrect approach to analyze the positional distribution of salient objects. To avoid this misleading phenomenon, in Fig. 4 (e), we plot the statistics of two quantities,  $r_o$  and  $r_m$ , which denote how far an object center and its farthest (margin) point are from the image center, respectively. Both  $r_o$  and  $r_m$  are divided by half the diagonal length of the image for normalization, such that  $r_o, r_m \in [0, 1]$ . From these statistics, we observe that the salient objects in our dataset do not suffer from center bias.

**5) Size of Salient Objects.** The size of an instance-level salient object is defined as the proportion of its pixels to those in the overall image [39]. As shown in Fig. 4 (f), the sizes of salient objects in our SOC vary greatly compared with the only other existing instance-level dataset, ILSO [61]. Further, there is a higher proportion of medium-sized objects in SOC.

**6) Salient Objects with Attributes.** Having attribute information for the images in a dataset helps objectively assess the performance of models over different types of parameters and variations. It also allows for the inspection of model failures. To this end, we define a set of attributes to represent specific situations encountered in real-world scenes, such as *motion blur*, *occlusion* and *cluttered background* (summarized in Table 5). Note that an

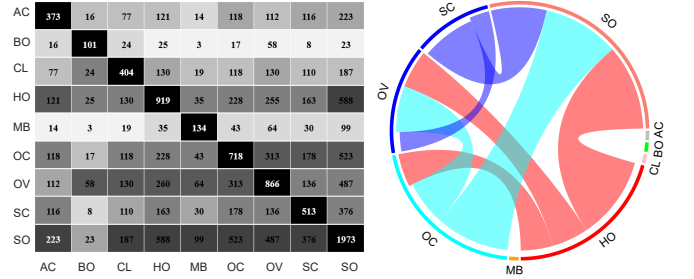


Figure 6. Left: Attribute distribution over salient object images in our SOC dataset. Each number in the grid indicates the number of occurrences. Right: The dominant dependencies among attributes based on the frequency of occurrences. A larger link width indicates a higher probability of an attribute occurring with other ones.

image can be annotated with multiple attributes as these attributes are not exclusive.

Inspired by [315], we present the distribution of attributes over the dataset in the left of Fig. 6. The *SO* attribute makes up the largest proportion due to our accurate instance-level annotations (*e.g.*, the tennis racket in Fig. 3). The *HO* attribute also accounts for a large proportion, because the real-world scenes are composed of different constituent materials. *Motion blur* (*MB*) is more common in video frames, but also sometimes occurs in still images. Thus, *MB* images make up a relatively small proportion of our dataset. Since a realistic image usually contains multiple attributes, we show the dominant dependencies among attributes based on the frequency of occurrence on the right of Fig. 6. For example, a scene containing several heterogeneous objects is likely to have a large number of objects occluding each other and forming complex spatial structures. Thus, the *HO* attribute has a strong dependency with *OC*, *OV*, and *SO*.

**7) High-Quality Salient Object Labeling.** As noted in [316], training on the ECSSD dataset (1,000 images) yields better results than when using other datasets (*e.g.*, MSRA10K with 10,000 images). This is because, besides the scale, dataset quality is also an important. To obtain a large number of high-quality images, we randomly selected images from the MS-COCO dataset [87], which is a large-scale real-world dataset whose objects are annotated with polygons (*i.e.*, coarse labeling). High-quality labels also play a critical role in improving the accuracy of SOD models [82]. Towards this end, we re-labeled the dataset with pixel-wise annotations. Following other famous task-oriented SOD benchmark datasets [32], [33], [34], [35], [37], [40], [41], [61], [82], [85], [86], we did not use an eye tracking device. We took two steps to ensure high-quality annotations: (i) We asked five viewers to annotate objects that they thought were salient in each image with bounding

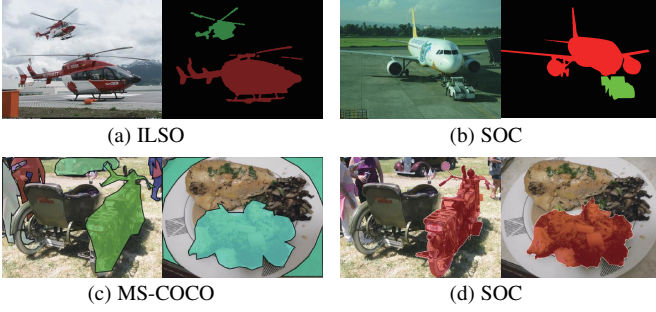


Figure 7. Compared with the recent instance-level ILSO dataset [61] (a), which is labeled with discontinuous coarse boundaries, and MS-COCO dataset [87] (c), which is labeled with polygons, our SOC dataset (b & d) is labeled with smooth fine boundaries.

boxes (bboxes), and (ii) we kept the images in which the majority ( $\geq 3$ ) of viewers annotated the same objects (IOU of the bbox  $> 0.8$ ). After this first stage, we had 3,000 salient object images annotated with bboxes. *In the second stage*, we further manually labeled accurate silhouettes of the salient objects according to the bboxes. Note that we had 10 volunteers involved in both steps to cross-check the quality of annotations. In the end, we kept 3,000 images with high-quality, instance-level labeled salient objects. As shown in Fig. 7 (b & d), the boundaries of our object labels are precise, sharp and smooth. During the annotation process, we also added some new categories (e.g., *computer monitor, hat, pillow*) that are not labeled in the MS-COCO dataset [87].

## 4 OUR DATASET-ENHANCEMENT STRATEGIES

Instead of focusing on designing a strong decoder for feature aggregation, we introduce three simple dataset-enhancement strategies to achieve better model generalization ability. We argue that the proposed strategies are easy to implement by all existing fully supervised SOD models, and yield good performance with little effort. Let us define the RGB saliency training dataset as  $D = \{x_i, y_i\}_{i=1}^N$ , where  $x_i, y_i$  are an input RGB image and its corresponding ground-truth (GT) saliency map,  $i$  indexes the training images, and  $N$  is the size of the training dataset. As SOD is a binary prediction task, the GT saliency map  $y$  is usually a binary map, and most existing SOD techniques employ a binary (or weighted) cross-entropy loss function to evaluate the saliency prediction. In this paper, instead of defining the GT saliency map as a binary segmentation map, we first introduce “label smoothing” [292] as an effective technique to achieve both efficient model training and high model performance. Then, we adopt random image augmentation to generate diverse samples for better model generalization ability. Finally, as a widely studied technique in semi-supervised or unsupervised learning [295], [307], we extend the self-supervised learning solution to fully supervised SOD to achieve a robust model.

### 4.1 Label Smoothing

**Label Smoothing and Knowledge Distillation.** One of the most important scenarios in which to apply label smoothing is the teacher-student net [317] for knowledge distillation. Typically, in a teacher-student net, the teacher model has a strong learning capacity, while the student model has a lower one. The teacher model then teaches the student model by providing the latter with a “soft target”. As discussed in [318], the “soft target” contains a rich similarity structure over the data, which is essential for

producing an enhanced student model. Further, label smoothing can be treated as a form of output distribution regularization that prevents the network from overfitting. As pointed out in [292], hard labels may lead to the overfitting as the model will assign full probability to each category, which is not guaranteed to generalize well. With soft labels, the model learns the structure of the data, thus preventing it from being over-confident. Following the same data setting, e.g., employing label smoothing, [319] introduced online label smoothing solution to gradually update the soft labels based on the model’s prediction.

**Conventional Setting.** Given an input image  $x$  and the corresponding ground-truth saliency map  $y$ , the conventional deep saliency model  $f_\theta$  is trained to achieve saliency prediction  $s = f_\theta(x)$  by minimizing the cross-entropy loss:  $\mathcal{L}_{ce}(y, s) = -\sum_{i=1}^N \sum_{u,v} y_i^{u,v} \log s_i^{u,v}$ , where  $(u, v)$  index pixels. For the hard label based framework, we have  $y \in \{0, 1\}$ , where 1 indicates the salient foreground and 0 represents the background.

**Label Smoothing Setting.** Different from the above hard label setting, in label smoothing regularization (LSR) [292], a smoothed label  $y'$  is used instead of  $y$ , which is formulated as:

$$y' = (1 - \varepsilon)y + \varepsilon u(x). \quad (1)$$

Here,  $\varepsilon$  is the smoothing parameter, and  $u(x)$  is a fixed distribution, which is usually defined as a uniform distribution. The smoothed label with a uniform distribution  $u(x)$  is then defined as:

$$y' = (1 - \varepsilon)y + \frac{\varepsilon}{K}, \quad (2)$$

where  $K$  is the number of categories.

**Loss Function.** Given smoothed label  $y'$  and hard label  $y$ , the loss function with LSR is defined as:

$$\mathcal{L}_{ls} = (1 - \alpha)\mathcal{L}_{ce}(y, s) + \alpha\mathcal{L}_{ce}(y', s), \quad (3)$$

where  $\alpha$  is used to balance the contribution of the smoothed and hard labels, and the smoothed label related loss is defined as  $\mathcal{L}_{lsr} = \mathcal{L}_{ce}(y', s)$ . Note that, if there exist other loss functions, the smoothed label can only be used in cross-entropy loss.

**What Does Label Smoothing Really Do?** The conventional cross-entropy loss can be rewritten as:

$$\mathcal{L}_{ce} = -\log s. \quad (4)$$

Here,  $s$  is the model prediction after sigmoid activation (for binary classification), which is defined as:

$$s_j = e^{z_j} / \sum_{k=1}^K e^{z_k} = 1 / (1 + \sum_{k \neq j} e^{z_k - z_j}). \quad (5)$$

We then substitute  $s$  in (Eq. 4) and obtain:

$$\mathcal{L}_{ce} = \log(1 + \sum_{k \neq j} e^{z_k - z_j}). \quad (6)$$

Let us define the gap between the correct class and others as  $M = z_k - z_j$ . We can then conclude that the conventional cross-entropy loss aims to maximize this gap.

For label smoothing setting, as in (Eq. 2), we rewrite the smoothed label related loss  $\mathcal{L}_{lsr}$  as:

$$\begin{aligned} \mathcal{L}_{lsr} &= -((1 - \varepsilon)y + \varepsilon/K) \log s - (1 - (1 - \varepsilon)y - \varepsilon/K) \log(1 - s) \\ &= -(y \log s + (1 - y) \log(1 - s)) + (\varepsilon y - \frac{\varepsilon}{K}) \log(\frac{s}{1 - s}). \end{aligned} \quad (7)$$

Using the definition of  $s$  in (Eq. 5), we have:

$$\frac{s_j}{1-s_j} = \frac{1}{\sum_{k=1}^K e^{z_k-z_j} - 1}. \quad (8)$$

We can then combine (Eq. 8) with (Eq. 7) and obtain:

$$\mathcal{L}_{lsr} = \mathcal{L}_{ce}(y, s) + (\epsilon y - \frac{\epsilon}{K}) * \frac{1}{\sum_{k=1}^K e^{z_k-z_j} - 1}. \quad (9)$$

The first part of (Eq. 9) aims to maximize the gap between the correct class and the others, which is same as the conventional binary-cross entropy loss as in (Eq. 6). The second part works in the opposite direction (compared with (Eq. 6)) to narrow the gap. In this way, the smoothed label related loss works to balance the gap between the correct class and others, which serves as an regularization to prevent the model from being over-confident.

## 4.2 Data Augmentation

As an effective data pre-processing technique, data augmentation aims to generate new samples from an existing dataset, thus producing a model with good generalization ability. Given the training dataset  $D = \{x_i, y_i\}_{i=1}^N$ , data augmentation produces a new dataset  $D' = \{x'_i, y'_i\}_{i=1}^{N'}$ . As discussed previously, two main types of data augmentation have received particular attention. These include the handcrafted policies and learned policies [301], [302]. For the learned policies, we observe that the augmented data can change drastically depending on the context, which may not be an issue for image classification, but will change the salient attributes of an image. We thus focus only on handcrafted policies.

For handcrafted data augmentation policies, existing works [303], [304], [305], [306] focus on three main directions: 1) image transformation, *e.g.*, scale or rotation transformation; 2) mix-up to generate new samples, which are neighbors of the existing samples; and 3) adding noise to the ground-truth. Similar to learned policies, the mix-up strategy change the context information of an image, which is harmful for context-based tasks, such as salient object detection. In this paper, we therefore focus on two very simple data augmentation techniques, namely image transformation and adding noise to the ground-truth. For image transformation, we randomly scale, rotate and crop part of the image (85% of the original image to keep the context information). For the additive noise solution, we randomly add Gaussian noise of distribution  $\mathcal{N}(0.1, 0.3)$  to the ground-truth saliency map, leading to a noisy ground-truth map. Note that, for image transformation, we transform image and ground-truth at the same time, while when adding noise to the ground-truth, we only process the ground-truth saliency maps.

## 4.3 Self-Supervised Learning

Self-supervised learning learns from an image without knowing the task itself or the ground-truth, making it an unsupervised representation learning technique. Conventionally, for the supervised learning setting, the loss function is defined as  $\mathcal{L}_{ce}(y, s)$ , where  $s$  is the model's prediction, and  $y$  is the ground-truth map. For self-supervised learning, the final loss function usually includes two main parts: the conventional cross-entropy loss  $\mathcal{L}_{ce}(y, s)$  and an unsupervised loss that serves as a regularizer, *i.e.*,  $\mathcal{L}(g(x), s)$ , where  $g(x)$  is the transformation of the original input image  $x$ . The two studies [295], [308] introduced a self-supervised loss with rotation estimation as a pretext task.

Similarly, we introduce a scale/rotation consistency loss function to achieve scale/rotation invariant predictions. Specifically,

given an input image  $x$ , we define its prediction as  $s$ . Then, we apply an image transformation (scale or rotation transformation) and obtain  $x'$ . We then perform the same transformation on the prediction  $s$  and obtain  $s'$ . We feed  $x'$  to the same salient object detection network to get the saliency prediction as  $s'$ . We assume that  $s'$  and  $s$  should be similar. Then, we adopt the single scale structural similarity index measure (SSIM) [320], [321] as a similarity measure, and define the self-supervised loss as:

$$\mathcal{L}_{ss} = 1 - SSIM(s', s). \quad (10)$$

## 4.4 Loss Function with the Proposed Strategies.

With the three introduced data-enhancement strategies, we first apply random data augmentation to both our training image set and training ground-truth set, as in Section 4.2. Then we generate the smoothed label following (Eq. 1), with  $K = 2$  in this paper to represent the salient foreground and background regions. In addition to the loss function in (Eq. 3), we also introduce a self-supervised loss  $\mathcal{L}_{ss}$ . Our final loss function is then defined as:

$$\mathcal{L} = \mathcal{L}_{ls} + \gamma \mathcal{L}_{ss}, \quad (11)$$

where  $\gamma$  is introduced to balance the self-supervised loss, and is empirically set to  $\gamma = 0.3$  in this paper.

## 5 SOC BENCHMARK

Based on three criteria (*i.e.*, representative pipeline, open-sourced, and state-of-the-art performance), we select 46 traditional SOD methods and 54 deep learning models from 201 reviewed methods (see § 2) to conduct our benchmark. To the best of our knowledge, this benchmark is the most comprehensive study in the RGB SOD.

### 5.1 Experimental Setup

#### 5.1.1 Evaluation Metrics

Note that the GTs of non-salient images in our SOC dataset are all-zero matrices, so directly using the traditional F-measure [82] will result in very low and inaccurate scores. Thus, we utilize three golden metrics (*i.e.*, MAE [322], maximum E-measure [4], and S-measure [3]) to avoid this issue and to provide a more reliable assessment. Our python evaluation toolboxes are now publicly available.<sup>5</sup>

- **MAE** ( $M$ ) is the mean absolute error metric, which is widely used to measure the pixel-level difference between the prediction and the GT.
- **E-measure** ( $E_{\xi}^{max}$ ) is a new perceptual metric that takes both local and global similarity into consideration.
- **S-measure** ( $S_{\alpha}$ ) is a standard metric that quantizes the structural similarity at a region and object level.

Table 6  
SOC dataset used in the benchmarking experiments.

	SOC_train	SOC_val	SOC_test	Total
Salient Objects (Sal)	1,800	600	600	3,000
Non-Salient Objects (NonSal)	1,800	600	600	3,000
Total	3,600	1,200	1,200	6,000

5. <https://github.com/mczhuge/SOCToolbox>.

Table 7

Comparison of the traditional SOD algorithms on our SOC\_test set (1,200 images) in terms of  $S_\alpha \uparrow$ ,  $E_\xi^{max} \uparrow$ , and  $M \downarrow$ . The top-3 results are highlighted in **red**, **blue** and **green**, respectively. The superscript of each score is the corresponding ranking. Details of these methods are summarized in Table 2. The overall rank index indicates the average ranking of the three metrics. These results are available at: [Google Drive](#).

	#	Model	Code	$S_\alpha \uparrow$	$E_\xi^{max} \uparrow$	$M \downarrow$	Rank
2014-before	1	SUN [96]	Matlab	0.475 <sup>46</sup>	0.688 <sup>44</sup>	0.436 <sup>46</sup>	46
	2	LSSC [107]	Matlab + C	0.552 <sup>45</sup>	0.714 <sup>43</sup>	0.365 <sup>45</sup>	45
	3	BSF [112]	Matlab	0.554 <sup>44</sup>	0.728 <sup>38</sup>	0.353 <sup>44</sup>	44
	4	GR [109]	Matlab + C	0.588 <sup>41</sup>	0.715 <sup>42</sup>	0.332 <sup>42</sup>	43
	5	HS [37]	EXE	0.601 <sup>40</sup>	0.729 <sup>37</sup>	0.321 <sup>41</sup>	42
	6	Itti [45]	Matlab	0.587 <sup>42</sup>	0.736 <sup>30</sup>	0.311 <sup>39</sup>	41
	7	AIM [95]	Matlab	0.605 <sup>39</sup>	0.670 <sup>45</sup>	0.250 <sup>24</sup>	39
	8	GBVS [93]	Matlab	0.615 <sup>36</sup>	0.733 <sup>35</sup>	0.293 <sup>37</sup>	39
	9	LR [116]	Matlab	0.642 <sup>31</sup>	0.723 <sup>40</sup>	0.253 <sup>27</sup>	36
	10	CA [323]	Matlab + C	0.606 <sup>38</sup>	0.750 <sup>22</sup>	0.291 <sup>36</sup>	35
	11	MR [38]	Matlab + C	0.645 <sup>29</sup>	0.734 <sup>33</sup>	0.259 <sup>31</sup>	32
	12	SEG [99]	Matlab + C	0.576 <sup>43</sup>	0.765 <sup>7</sup>	0.352 <sup>43</sup>	32
	13	FT [82]	C	0.626 <sup>34</sup>	0.738 <sup>29</sup>	0.236 <sup>20</sup>	28
	14	MC [125]	Matlab + C	0.656 <sup>23</sup>	0.736 <sup>30</sup>	0.251 <sup>25</sup>	26
	15	CB [134]	Matlab + C	0.653 <sup>25</sup>	0.758 <sup>13</sup>	0.268 <sup>33</sup>	23
	16	SR [94]	Matlab/C++	0.658 <sup>21</sup>	0.661 <sup>46</sup>	0.156 <sup>4</sup>	23
	17	PCA [117]	Matlab + C	0.670 <sup>18</sup>	0.741 <sup>28</sup>	0.209 <sup>13</sup>	17
	18	MSS [110]	Matlab	0.682 <sup>12</sup>	0.776 <sup>4</sup>	0.231 <sup>19</sup>	10
	19	SF [113]	C	0.699 <sup>6</sup>	0.747 <sup>26</sup>	<b>0.130</b> <sup>1</sup>	8
	20	DSR [124]	Matlab + C	0.702 <sup>5</sup>	0.751 <sup>20</sup>	0.184 <sup>8</sup>	8
	21	MSSS [100]	C	0.683 <sup>11</sup>	0.757 <sup>14</sup>	0.164 <sup>5</sup>	7
	22	HDCT [118]	Matlab	0.696 <sup>7</sup>	0.774 <sup>5</sup>	0.201 <sup>12</sup>	6
	23	DRFI [114]	C	0.709 <sup>4</sup>	<b>0.791</b> <sup>2</sup>	0.197 <sup>11</sup>	4
	24	COV [108]	Matlab	<b>0.711</b> <sup>3</sup>	0.761 <sup>9</sup>	<b>0.146</b> <sup>2</sup>	2
	25	RBD [115]	Matlab	<b>0.716</b> <sup>2</sup>	<b>0.784</b> <sup>3</sup>	0.186 <sup>9</sup>	2
2021-2015	26	WMR [324]	Matlab + C	0.640 <sup>32</sup>	0.733 <sup>35</sup>	0.269 <sup>34</sup>	38
	27	MAPM [142]	Matlab + C	0.644 <sup>30</sup>	0.722 <sup>41</sup>	0.256 <sup>29</sup>	37
	28	BL [156]	Matlab + C	0.623 <sup>35</sup>	0.751 <sup>20</sup>	0.296 <sup>38</sup>	32
	29	RRWR [159]	Matlab	0.647 <sup>27</sup>	0.735 <sup>32</sup>	0.258 <sup>30</sup>	31
	30	WLRR [325]	Matlab + C	0.614 <sup>37</sup>	0.759 <sup>11</sup>	0.312 <sup>40</sup>	30
	31	RCRR [144]	Matlab	0.650 <sup>26</sup>	0.734 <sup>33</sup>	0.255 <sup>28</sup>	29
	32	GP [153]	Matlab + C	0.632 <sup>33</sup>	0.759 <sup>11</sup>	0.287 <sup>35</sup>	27
	33	TLLT [160]	Matlab	0.656 <sup>23</sup>	0.725 <sup>39</sup>	0.214 <sup>15</sup>	25
	34	BSCA [154]	Matlab + C	0.657 <sup>22</sup>	0.755 <sup>16</sup>	0.259 <sup>31</sup>	22
	35	SMD [136]	Matlab	0.662 <sup>20</sup>	0.748 <sup>25</sup>	0.246 <sup>22</sup>	21
	36	MDC [147]	C	0.675 <sup>16</sup>	0.744 <sup>27</sup>	0.219 <sup>17</sup>	20
	37	DSP [140]	Matlab + C	0.664 <sup>19</sup>	0.754 <sup>17</sup>	0.248 <sup>23</sup>	17
	38	MIL [143]	Matlab + C	0.671 <sup>17</sup>	0.750 <sup>22</sup>	0.236 <sup>20</sup>	17
	39	MST [158]	C	0.647 <sup>27</sup>	0.773 <sup>6</sup>	0.251 <sup>25</sup>	16
	40	GLC [139]	Matlab + C	0.676 <sup>15</sup>	0.756 <sup>15</sup>	0.223 <sup>18</sup>	15
	41	MBS [152]	Matlab	0.678 <sup>14</sup>	0.753 <sup>18</sup>	0.214 <sup>15</sup>	14
	42	LPS [141]	Matlab + C	0.694 <sup>9</sup>	0.749 <sup>24</sup>	0.183 <sup>7</sup>	13
	43	WFD [326]	C	0.680 <sup>13</sup>	0.760 <sup>10</sup>	0.213 <sup>14</sup>	12
	44	BFS [138]	Matlab + C	0.696 <sup>7</sup>	0.753 <sup>18</sup>	0.195 <sup>10</sup>	10
	45	WSC [161]	Matlab	0.693 <sup>10</sup>	0.765 <sup>7</sup>	0.179 <sup>6</sup>	5
	46	HCCH [148]	Matlab	<b>0.736</b> <sup>1</sup>	<b>0.794</b> <sup>1</sup>	<b>0.149</b> <sup>3</sup>	1

### 5.1.2 Training and Testing Protocols

The statistics of the SOC dataset used in the benchmark are summarized in Table 6. For traditional algorithms, we directly test their performance on the SOC-test set (1,200 images). For deep learning models, we first adopt the pre-trained models with their recommended training parameter settings under the default training dataset (see Tables 3 & 4) and then evaluate them on the SOC\_test set to roughly obtain the top-100 models (see Table 7 & 8). Finally, we provide a quantitative comparison and detailed analysis of 15 SOTA approaches, including the top-5 traditional methods and top-10 deep learning models.

## 5.2 Quantitative Comparisons

To build a standardized leaderboard (*i.e.*, same image resolution, thresholding step, and evaluation tool), we provide three golden metrics, *i.e.*,  $S_\alpha$ ,  $E_\xi^{max}$ , and  $M$ .

Table 7 shows the performance of 46 SOTA traditional SOD algorithms on our SOC\_test set. In terms of both **S-measure** (*i.e.*,  $S_\alpha$ ) and max **E-measure** ( $E_\xi^{max}$ ), the HCCH method surpasses all competitors by a large margin. RBD, COV, and DRFI obtain comparable performance in terms of  $S_\alpha$  score. Meanwhile, COV ranks third in terms of  $S_\alpha$  measure, but ninth in  $E_\xi^{max}$ . In terms

Table 8

Evaluation of 54 deep learning based SOD models on our SOC\_test set (1,200 images). We adopt the default implementations listed in Table 3 and Table 4 to test their generalization capability. These results are available at: [Google Drive](#).

	#	Model	Code	$S_\alpha \uparrow$	$E_\xi^{max} \uparrow$	$M \downarrow$	Rank
2015	1	LEGS [175]	Caffe	0.679 <sup>53</sup>	0.765 <sup>54</sup>	0.228 <sup>53</sup>	54
	2	MDF [40]	Caffe	0.739 <sup>49</sup>	0.768 <sup>53</sup>	0.144 <sup>43</sup>	49
	3	MC [176]	Caffe	0.757 <sup>47</sup>	0.823 <sup>43</sup>	0.138 <sup>35</sup>	43
2016	4	DSL [178]	Caffe	0.724 <sup>52</sup>	0.810 <sup>47</sup>	0.194 <sup>52</sup>	51
	5	DISC [180]	Caffe	0.735 <sup>51</sup>	0.810 <sup>47</sup>	0.175 <sup>50</sup>	50
	6	DCL [194]	Caffe	0.771 <sup>44</sup>	0.836 <sup>39</sup>	0.157 <sup>48</sup>	45
	7	ELD [193]	Caffe	0.774 <sup>42</sup>	0.836 <sup>39</sup>	0.138 <sup>35</sup>	40
	8	DS [181]	Caffe	0.779 <sup>40</sup>	0.860 <sup>24</sup>	0.155 <sup>46</sup>	37
	9	DHS [168]	Pytorch	0.800 <sup>32</sup>	0.848 <sup>33</sup>	0.122 <sup>30</sup>	33
	10	RFCN [186]	Caffe	0.814 <sup>23</sup>	0.858 <sup>27</sup>	0.113 <sup>23</sup>	25
2017	11	UCF [203]	Caffe	0.654 <sup>54</sup>	0.805 <sup>51</sup>	0.285 <sup>54</sup>	53
	12	AMU [204]	Caffe	0.737 <sup>50</sup>	0.808 <sup>50</sup>	0.185 <sup>51</sup>	51
	13	SVF [202]	Caffe	0.761 <sup>45</sup>	0.816 <sup>45</sup>	0.156 <sup>47</sup>	47
	14	WSS [41]	Caffe	0.778 <sup>41</sup>	0.821 <sup>44</sup>	0.140 <sup>39</sup>	42
	15	DSS [200]	Caffe	0.807 <sup>30</sup>	0.858 <sup>27</sup>	0.111 <sup>20</sup>	27
	16	SRM [196]	Caffe	0.822 <sup>16</sup>	0.859 <sup>26</sup>	0.111 <sup>20</sup>	21
	17	MSRNet [61]	Caffe	0.816 <sup>19</sup>	0.871 <sup>16</sup>	0.117 <sup>25</sup>	20
	18	NLDF [198]	Tensorflow	0.816 <sup>19</sup>	0.860 <sup>24</sup>	0.104 <sup>13</sup>	16
2018	19	RAS [212]	Pytorch	0.759 <sup>46</sup>	0.813 <sup>46</sup>	0.151 <sup>44</sup>	46
	20	R3Net [209]	Pytorch	0.773 <sup>43</sup>	0.825 <sup>42</sup>	0.138 <sup>35</sup>	41
	21	LPSNet [213]	Pytorch	0.795 <sup>35</sup>	0.838 <sup>38</sup>	0.143 <sup>42</sup>	39
	22	DGRL-GLN [217]	Caffe	0.794 <sup>36</sup>	0.845 <sup>36</sup>	0.141 <sup>40</sup>	38
	23	C2SNet [211]	Caffe	0.791 <sup>37</sup>	0.845 <sup>36</sup>	0.138 <sup>35</sup>	36
	24	PiCA-Res [218]	Pytorch	0.810 <sup>28</sup>	0.858 <sup>27</sup>	0.128 <sup>31</sup>	31
	25	BMPM [216]	Tensorflow	0.810 <sup>28</sup>	0.853 <sup>30</sup>	0.119 <sup>27</sup>	29
	26	ASNet [215]	Keras	0.817 <sup>18</sup>	0.865 <sup>20</sup>	0.111 <sup>20</sup>	17
	2019	27	MWS [236]	Pytorch	0.757 <sup>47</sup>	0.828 <sup>41</sup>	0.172 <sup>49</sup>
28		AFNet [239]	Caffe	0.812 <sup>24</sup>	0.850 <sup>32</sup>	0.120 <sup>29</sup>	29
29		SIBA [249]	Caffe	0.800 <sup>32</sup>	0.884 <sup>10</sup>	0.130 <sup>33</sup>	26
30		Deepside [233]	Caffe	0.815 <sup>21</sup>	0.861 <sup>23</sup>	0.119 <sup>27</sup>	24
31		PFANet [240]	Tensorflow	0.815 <sup>21</sup>	0.846 <sup>35</sup>	0.101 <sup>8</sup>	22
32		PoolNet [243]	Pytorch	0.829 <sup>13</sup>	0.868 <sup>18</sup>	0.106 <sup>16</sup>	14
33		SCRNet [44]	Pytorch	0.833 <sup>11</sup>	0.872 <sup>15</sup>	0.105 <sup>14</sup>	13
34		CPDVgg [242]	Pytorch	<b>0.856</b> <sup>1</sup>	0.889 <sup>6</sup>	<b>0.079</b> <sup>2</sup>	2
35		EGNet [250]	Pytorch	<b>0.858</b> <sup>1</sup>	<b>0.896</b> <sup>2</sup>	<b>0.078</b> <sup>1</sup>	1
2020		36	ABPNet [282]	Pytorch	0.783 <sup>38</sup>	0.810 <sup>47</sup>	0.153 <sup>45</sup>
	37	U2Net [273]	Pytorch	0.780 <sup>39</sup>	0.795 <sup>52</sup>	0.105 <sup>14</sup>	35
	38	GCPANet [277]	Pytorch	0.807 <sup>30</sup>	0.848 <sup>33</sup>	0.133 <sup>34</sup>	34
	39	ITSD [280]	Pytorch	0.798 <sup>34</sup>	0.870 <sup>17</sup>	0.142 <sup>41</sup>	32
	40	MINet [281]	Pytorch	0.819 <sup>17</sup>	0.864 <sup>22</sup>	0.117 <sup>25</sup>	22
	41	SANet [56]	Pytorch	0.812 <sup>24</sup>	0.868 <sup>18</sup>	0.106 <sup>16</sup>	17
	42	GateNetVgg [284]	Pytorch	0.827 <sup>15</sup>	0.865 <sup>20</sup>	0.108 <sup>18</sup>	15
	43	F3Net [278]	Pytorch	0.828 <sup>14</sup>	0.891 <sup>5</sup>	0.109 <sup>19</sup>	12
	44	CSNet [283]	Pytorch	0.834 <sup>10</sup>	0.876 <sup>14</sup>	0.103 <sup>10</sup>	11
	45	LDF [279]	Pytorch	0.835 <sup>9</sup>	0.878 <sup>12</sup>	0.103 <sup>10</sup>	10
	46	RASNet [258]	Pytorch	0.832 <sup>12</sup>	0.887 <sup>8</sup>	0.103 <sup>10</sup>	9
	47	CAGVgg [271]	Keras	0.837 <sup>8</sup>	0.878 <sup>12</sup>	0.088 <sup>4</sup>	8
	48	DFI [254]	Pytorch	0.838 <sup>7</sup>	<b>0.903</b> <sup>1</sup>	0.101 <sup>8</sup>	5
49	R2Net [255]	Pytorch	<b>0.857</b> <sup>2</sup>	0.885 <sup>9</sup>	<b>0.084</b> <sup>3</sup>	4	
2021	50	SCWS [288]	Pytorch	0.811 <sup>26</sup>	0.851 <sup>31</sup>	0.115 <sup>24</sup>	28
	51	ICON [52]	Pytorch	0.811 <sup>26</sup>	<b>0.896</b> <sup>2</sup>	0.128 <sup>31</sup>	19
	52	BAS [31]	Pytorch	0.842 <sup>5</sup>	0.882 <sup>11</sup>	0.092 <sup>7</sup>	7
	53	ABP [327]	Pytorch	0.842 <sup>5</sup>	0.889 <sup>6</sup>	0.091 <sup>6</sup>	6
	54	CVAE [327]	Pytorch	0.849 <sup>4</sup>	<b>0.892</b> <sup>4</sup>	0.089 <sup>5</sup>	3

of MAE (*i.e.*,  $M$ ), the top-5 approaches are: SF, COV, HCCH, SR, and MSSS. It is worth mentioning that SF reduces  $M$  and outperforms all the recent traditional SOD methods. Based on their overall scores, the top-5 methods are HCCH, RBD, COV, DRFI, and WSC.

The quantitative results of the 54 deep learning SOD models on our SOC\_test dataset are shown in Table 8. In terms of  $S_\alpha$ , EGNet, R2Net, and CPDVgg are the top-3 models, with scores of more than 0.85. Roughly 46% (*i.e.*, 21/45) of model scores are between 0.650 and 0.800. Compared with the traditional model, which achieves an  $S_\alpha$  score of 0.736, we can see continuous improvement over the past few years, with the exception of four early models (*i.e.*, DISC, DSL, LEGS, and UCF). At the same time, 30 out of 45 models achieve high performance (*e.g.*,  $0.800 \leq S_\alpha \leq 0.850$ ) and the average performance is nearly 0.820. Interestingly, in terms of

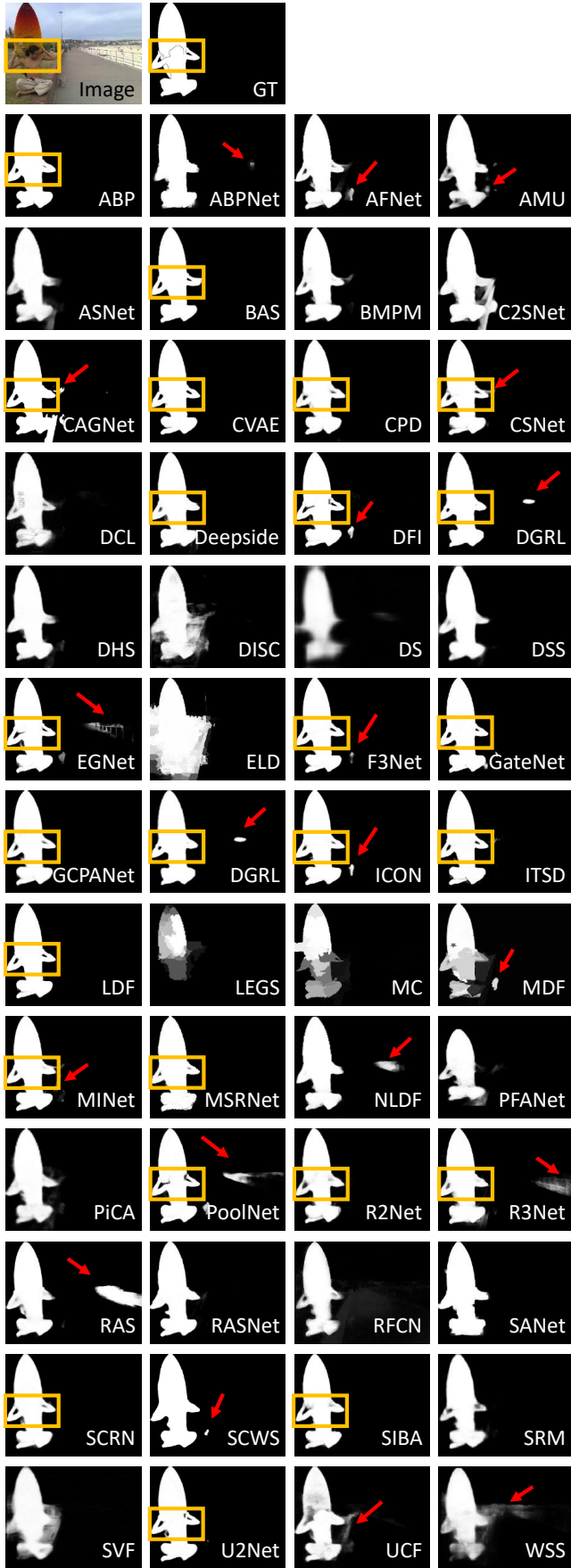


Figure 8. Visualization results of deep learning models.

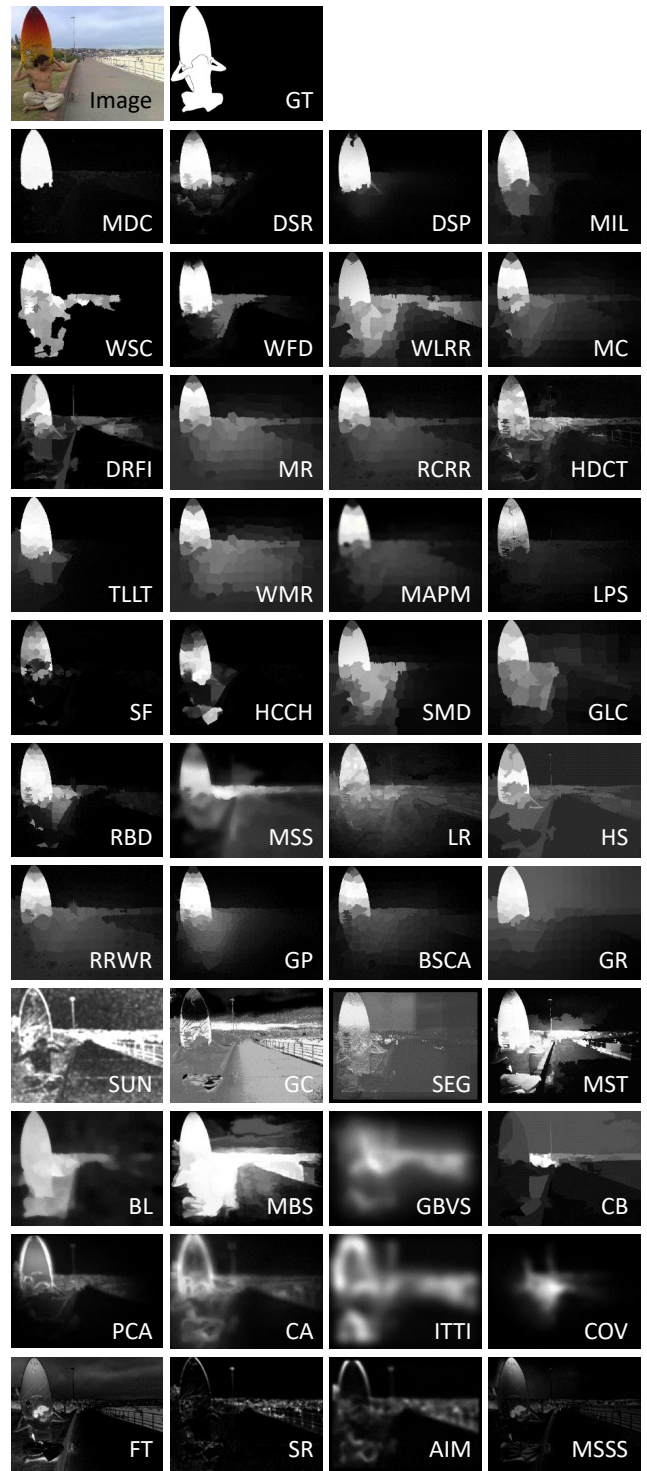


Figure 9. Qualitative results of state-of-the-art traditional approaches.

$E_{\xi}^{max}$ , the multi-task learning framework DFI and integrity learning model have the best and second-best scores of 0.903 and 0.896, respectively. Consistent with S-measure, in terms of MAE, we obtain the same top-3 models EGNNet, CPDVgg, and R2Net. From our 54 benchmarked models, we find that models that perform well in terms of S-measure also do well in MAE. Overall, the top-10 approaches are EGNNet, CPDVgg, CVAE, R2Net, DFI, ABP, BAS, CAGVgg, RASNet, and LDF. In the following section (§ 6), we will provide a more detailed analysis of these models.

Table 9  
Comparison of 14 state-of-the-art approaches in terms of attribute-level performance. For deep learning models, we re-train them on our SOC-Sal\_train set (*i.e.*, 1,800 images). Please refer to Tables 2, 3, & 4 for more details. These results are available at: [Google Drive](#).

	Attribute Model	AC		BO		CL		HO		MB		OC		OV		SC		SO		Avg.	
		$S_\alpha \uparrow$	$M \downarrow$																		
Traditional	COV [108]	0.505	0.216	0.277	0.577	0.453	0.280	0.508	0.229	0.494	0.219	0.484	0.246	0.423	0.314	0.535	0.174	0.525	0.172	0.467	0.270
	WSC [161]	0.541	0.205	0.356	0.517	0.517	0.252	0.556	0.211	0.536	0.210	0.529	0.227	0.475	0.292	0.567	0.170	0.535	0.181	0.512	0.252
	HCCH [148]	0.585	0.199	0.354	0.525	0.537	0.254	0.615	0.197	0.547	0.202	0.552	0.225	0.468	0.298	0.595	0.165	0.588	0.162	0.538	0.247
	DRFI [114]	0.598	0.229	0.391	0.513	0.570	0.274	0.618	0.230	0.556	0.230	0.577	0.248	0.527	0.304	0.614	0.188	0.585	0.197	0.560	0.268
	RBD [115]	0.589	0.225	0.429	0.481	0.575	0.260	0.625	0.216	0.557	0.213	0.583	0.235	0.521	0.295	0.602	0.191	0.579	0.192	0.562	0.256
Deep Learning	ABP [327]	0.767	0.092	0.592	0.315	0.742	0.125	0.787	0.101	0.742	0.095	0.740	0.112	0.746	0.132	0.759	0.083	0.741	0.080	0.735	0.126
	EGNet [250]	0.791	0.088	0.593	0.307	0.739	0.137	0.788	0.110	0.763	0.115	0.743	0.120	0.750	0.138	0.800	0.076	0.753	0.088	0.747	0.131
	CPDVgg [242]	0.806	0.076	0.626	0.278	0.765	0.118	0.808	0.096	0.786	0.097	0.765	0.103	0.760	0.127	0.801	0.070	0.765	0.076	0.765	0.116
	CAGVgg [271]	0.795	0.080	<b>0.700</b>	<b>0.208</b>	0.782	0.115	0.808	0.098	0.764	0.102	0.751	0.120	0.763	0.127	0.795	0.081	0.744	0.093	0.767	0.114
	RASNet [258]	<b>0.821</b>	<b>0.066</b>	0.626	0.276	0.785	<b>0.106</b>	<b>0.816</b>	<b>0.087</b>	0.788	<b>0.086</b>	0.776	<b>0.096</b>	0.779	<b>0.113</b>	<b>0.810</b>	<b>0.066</b>	0.774	<b>0.070</b>	0.772	0.107
	CVAE [327]	0.813	0.075	0.688	0.217	<b>0.790</b>	<b>0.107</b>	<b>0.816</b>	<b>0.092</b>	0.784	0.091	0.771	0.104	0.776	0.115	<b>0.820</b>	<b>0.069</b>	0.767	0.080	<b>0.781</b>	<b>0.106</b>
	LDF [279]	0.819	<b>0.071</b>	<b>0.697</b>	<b>0.212</b>	<b>0.796</b>	<b>0.105</b>	<b>0.824</b>	<b>0.088</b>	<b>0.792</b>	<b>0.085</b>	<b>0.781</b>	<b>0.098</b>	<b>0.790</b>	<b>0.107</b>	0.780	0.073	<b>0.801</b>	<b>0.072</b>	<b>0.787</b>	<b>0.101</b>
	R2Net [255]	<b>0.827</b>	<b>0.071</b>	0.656	0.257	<b>0.802</b>	<b>0.107</b>	<b>0.826</b>	<b>0.092</b>	<b>0.794</b>	0.097	<b>0.789</b>	<b>0.099</b>	<b>0.791</b>	<b>0.112</b>	<b>0.807</b>	0.072	<b>0.788</b>	<b>0.073</b>	<b>0.787</b>	0.109
	BAS [31]	<b>0.831</b>	<b>0.060</b>	<b>0.723</b>	<b>0.166</b>	0.785	0.110	0.814	0.093	<b>0.797</b>	<b>0.072</b>	<b>0.780</b>	0.101	<b>0.781</b>	0.114	<b>0.820</b>	0.072	<b>0.787</b>	0.075	<b>0.791</b>	<b>0.096</b>
	Avg.	0.721	0.125	0.551	0.346	0.688	0.168	0.729	0.139	0.693	0.137	0.687	0.152	0.668	0.185	0.722	0.111	0.693	0.115	-	-

### 5.3 Qualitative Comparisons

Two qualitative comparisons are presented in Fig. 8 and Fig. 9. As can be seen from Fig. 8, deep models generate saliency maps that are similar to the GTs, to varying degrees. Specifically, for ASNet, C2SNet, BMPM, DCL, DHS, DSS, DS, DISC, SVF, RFCN, and PFANet, the position of the object can be well-identified. However, all these methods generate blurred responses on object boundaries. PFANet, MDF, MC and LEGS even nearly destroy the integrity of the object. To better highlight these results, we introduce yellow rectangles to mark the high-quality segmentation regions and utilize red arrows to point out the errors. We observe that eight models (ABPNet, AFNet, AMU, NLDF, RAS, SCWS, UCF, and WSS) can localize the human object but introduce additional noise. We also notice that CAGNet, CSNet, MINet, DGRL, EGNet, F3Net, ICON, PoolNet, and R3Net can even capture the small structure of the human elbow. Moreover, saliency maps from R2Net, Deepside, SIBA, and MSRNet demonstrate better results than the above-mentioned methods. Amazingly, BAS, U2Net, ABP, CPD, GateNet, GCPANet, ITSD, LDF, SCRNet, and CAVE perform very close to the GT and result in knife-edge-shaped boundaries in the yellow rectangle region without any additional noise.

In sharp contrast to the deep learning models, the traditional models (Fig. 9) all fail without exception. WSC, HCCH, and RBD are the three most promising approaches. However, their results are still far from the GT map, since they are mainly based on various prior features extracted from color, orientation, contrast, *etc.* Further, the center bias prior is not suitable in this case, since the human is located close to the image boundary, thus making this example more challenging for these approaches.

## 6 FURTHER BENCHMARKING

### 6.1 Attribute-Based Evaluation

Based on the top-ranked models presented in Tables 7 & 8, we further re-train the top-10<sup>6</sup> deep learning models (using their default settings) on the SOC-Sal\_train set (1,800 images) and then test them on the SOC-Sal\_test set for attribute-based evaluation. In Table 9, we show the performance on subsets of our dataset characterized by a particular attribute. Due to space limitations,

in the following discussion, we only select a few representative attributes for further analysis.

*Big object* (BO) scenes typically occur when objects are close to the camera, enabling tiny text and patterns to be seen clearly. In this case, models that prefer to focus on local information are seriously misled, leading to a considerable decrease in performance (*e.g.*, 8.6%  $S_\alpha$  reduction for BAS, 8.7% reduction for CAGVgg, 11.4% reduction for LDF, and 40.7% reduction for COV) compared with their average performance (Avg.). Among all attributes, BOs are the most difficult for both traditional and deep learning models.

*Small objects* (SOs) are tricky for some SOD models. Four models (*i.e.*, BAS, CVAE, CAGVgg, and RASNet) encounter performance degradation (*e.g.*, from BAS-0.5% to RASNet-3.6%) because SOs are easily ignored during the downsampling of CNNs. Other models instead have enhanced performance on SOs, but significant reduction in performance on BOs.

*Heterogeneous objects* (HOs) commonly appear in natural scenes. The performance of all models on HOs improves to some degree, fluctuating from 2.9% to 14.3%. We suspect this is because, as shown in Fig. 6, HO images make up a significant proportion of all datasets, so the models are more familiar with this attribute.

*Occlusion* (OC) scenes occur when objects are partly obscured. Thus, SOD models must capture global semantics to make up for the incomplete information of objects. As observed, traditional models obtain improved performance compared with their average performance. For deep learning models, in contrast, this situation is reversed.

As can be seen in the last row of Table 9 (average performance of each attribute), *MB* and *SO* have the same  $S_\alpha$  score. Moreover, the average scores of *AC* and *SC* are very similar. It seems that existing deep learning based SOD models can effectively address appearance change and shape complexity. Similar to the attributes of *OV* and *OC*, *CL* and *MB* remain challenging for existing methods, generating mid-level (*i.e.*,  $0.65 < S_\alpha < 0.70$ ) S-measure scores.

### 6.2 Comparison with Baselines

We introduce three dataset-enhancement strategies to prevent networks from being overconfident as a result of dataset bias. These include label smoothing, random data augmentation and self-supervised learning. We argue that our strategies can be easily used in existing salient object detection frameworks as general data processing techniques. We thus introduce our strategies to

6. The authors of DFI have only released the test code, so we only evaluate nine models.

Table 10  
The contribution of our dataset-enhancement strategies.

Metric \ Method	$S_\alpha \uparrow$	$E_\xi^{max} \uparrow$	$M \downarrow$
RASNet [258]	0.832	0.887	0.103
Our-RASNet	<b>0.841</b>	<b>0.897</b>	<b>0.096</b>
LDF [279]	0.835	0.878	0.103
Our-LDF	<b>0.845</b>	<b>0.891</b>	<b>0.097</b>
BAS [31]	0.842	0.882	0.092
Our-BAS	<b>0.856</b>	<b>0.895</b>	<b>0.086</b>
R2Net [255]	0.857	0.885	0.084
Our-R2Net	<b>0.868</b>	<b>0.899</b>	<b>0.080</b>
CVAE [327]	0.849	0.892	0.089
Our-CVAE	<b>0.863</b>	<b>0.902</b>	<b>0.086</b>

Table 11  
The contribution of each dataset-enhancement strategy.

Metric \ Method	$S_\alpha \uparrow$	$E_\xi^{max} \uparrow$	$M \downarrow$
CVAE [327]	0.849	0.892	0.089
LS	0.851	0.895	0.088
SS	0.852	0.894	0.088
RDA	0.855	0.896	0.086
Our-CVAE	<b>0.863</b>	<b>0.902</b>	<b>0.086</b>

Table 12  
Results for cross-dataset generalization in § 6. UC-Net (CVPR’20) [328] is trained on one dataset and tested on all others. “Sel.”: diagonal score (training and testing on the same dataset). “Oth.”: mean score on all except for self.

Measure	$S_\alpha \uparrow$ [3]								Drop↓	
Train \ Test	SOC	M10K	DU-O	DUTS	ECC	HKU	ILSO	Sel.	Oth.	
SOC [1]	<b>.884</b>	.768	.686	.834	.749	.774	.841	.884	.775	12%
M10K [35]	.800	<b>.921</b>	.784	.894	.881	.882	.884	.921	.854	7%
DU-O [38]	.833	.898	<b>.854</b>	.877	.862	.867	.886	.854	.871	-2%
DUTS [41]	.795	.882	.793	<b>.910</b>	.890	.903	.900	.910	.861	5%
ECC [37]	.791	.886	.800	.901	<b>.901</b>	.898	.903	.901	.863	4%
HKU [40]	.818	.892	.787	.904	.883	<b>.910</b>	.905	.910	.865	5%
ILSO [61]	.841	.888	.790	.898	.882	.896	<b>.920</b>	.920	.866	6%
Oth.	.813	.869	.773	.885	.858	.870	.887			

five benchmark salient object detection models and show the performance in Table 10, where “Our-” represents the benchmark models with our dataset-enhancement strategies. Further, we investigate the contribution of each data-enhancement strategy, and show the performance in Table 11, where we choose CVAE [327] as the base model.

**Training & Testing Protocols.** We retrain the five models in Table 10 with their corresponding training dataset, *e.g.*, MB [32] for RASNet [258], and DUTS [41] for all the other four models. We follow their original training and testing settings, *e.g.*, same maximum epoch, learning rate, training and testing image sizes.

**Discussion.** Table 10 shows consistent better performance of models with our strategies, which illustrates effectiveness of our solutions. Further, in Table 11, “LS”, “RDA”, “SS” represent adding label smoothing strategy, random data augmentation and self-supervised learning to the base model respectively. It shows that the random data augmentation achieves the largest performance gain, while label smoothing and self-supervised learning achieves comparable performance improvement. The main reason is that data augmentation introduce diverse samples to the initial training dataset, which is effective in improving model generalization ability. For the self-supervised learning strategy, as the CVAE model [327] has already adopt the multi-scale image as input strategy, we observe slightly improved performance. However, the

better performance in general can still validate the effectiveness of the proposed strategy. Label smoothing [292] was introduced to prevent model from over-confidence, thus achieve well-calibrated model. However, there exists no saliency metrics to explain the calibration error of the saliency models. We will investigate in expected calibration error [329] and extend it to saliency detection task in the future to better explain the calibration error of saliency models.

### 6.3 Cross-Dataset Generalization

To study the difficulty of existing SOD datasets, we adopt the CDA (cross-data analysis) method [43]. Given  $N$  candidate datasets  $\{D^n\}_{n=1}^N$ , we first train a model on the  $D_i$  dataset, and then test it on the other datasets (*i.e.*,  $\{D^m\}_{n=1, n \neq i}^N$ ). Following [76], [330], we randomly select 800 images and 200 images from each dataset as the training set and testing set, respectively.

We train UC-Net [328] on popular existing datasets that contain more than 1,000 images. Table 12 shows the  $S_\alpha$  score on each dataset. Each column provides the score of UC-Net tested on a specific dataset and trained on all others. Each row indicates the performance of UC-Net trained on one dataset and tested on all others, demonstrating the generalizability of the dataset adopted for training. We find that our SOC (*e.g.*, Oth. = 0.813) and DU-O (Oth. = 0.773) datasets are more difficult than other datasets. In addition, we notice that the model trained on our SOC dataset cannot perform well (*e.g.*, the Oth. column: 0.775) on other datasets. This is because our SOC dataset contains many real-world salient objects in open environments, thus the model cannot overfit the simple or clean scenes in existing datasets. This is also supported by our core observation that data selection bias is common in existing datasets.

## 7 FUTURE DIRECTIONS

Human attention can be influenced by four key factors:

- **Visual properties.** Our attention may be drawn by basic objects’ unique visual properties [331].
- **Memory.** If one knows an object well, it is easier for that object to attract one’s attention.
- **Goal.** For example, eye fixation records are quite different from attention maps, with a specific goal for viewers.
- **Emotion.** In addition to the above-mentioned factors, we argue that human attention toward the same scene may be affected by one’s emotion, *e.g.*, happiness, sadness, anger.

As demonstrated by Cave [331], attentional control is determined by a combination of these factors. Unfortunately, the annotations of existing SOD datasets do not clearly describe which factor they address. Differently, the ground-truth annotations of our SOC are based on the salicon (free-view task) dataset<sup>7</sup>, or so-call meaning maps which are used in recent studies [331], [332], [333]. As concluded by Kalash *et al.* [66], the work to date has addressed a relatively ill-posed problem. Thus, we recommend several future directions to re-think SOD tasks at six main research levels:

(1) **Data Level:** Recently, visual saliency detection tasks have attracted significant interest using 2D (RGB SOD) and 3D (*i.e.*, RGB-D, RGB-T) input data. However, light field SOD (4D), LIDAR SOD, and 360° SOD are still not well-studied. Establishing new datasets for these types of data will largely promote the development of this field. Another interesting avenue for examining

7. <http://salicon.net/>

saliency detection is to study fine-grained tasks, such as salient instance detection [61], [62], [334], [335] and part-object visual saliency detection [336].

(2) **Task Level:** Multi-task learning has demonstrated strong performance in recent works [337]. Existing schemes mainly focus on vision tasks, such as joint salient object detection and camouflaged object detection [338], detection of salient objects, edges and skeletons simultaneously [254], and simultaneous detection, ranking, and subitizing of multiple salient objects [64]. With the success of the transformer technique in natural language processing (NLP), introducing multi-modality learning into the saliency detection field may be a feasible way to further incorporate other types of information, such as CV+NLP (similar to [339]), CV+Audio [340], and CV+other modality.

(2) **Model Level:** A huge number of algorithms have been developed to improve detection accuracy. However, there are several promising directions that could be further studied such as data augmentation techniques [341], efficient SOD models (e.g., lightweight models [283], [342]), new loss functions [286], [343], ranking-based models [64], [137], and transformer-based models [344], [345].

(4) **Supervision Level:** In addition to the most common fully supervised learning of current SOD models, other supervision strategies, e.g., weakly supervised (i.e., scribble [56], category [346], and polygon), semi-supervised [53], self-supervised [60], [347], and unsupervised [58] learning are also interesting to study.

(5) **Evaluation Level:** Evaluation metrics are important for model training, testing, and benchmarking. However, the SOD community still utilizes classical metrics such as IoU, F-measure, and MAE. These metrics were designed for universal evaluation rather than for assessing SOD tasks specifically. As a consequence, they do not work well for certain specific applications, such as those with high-quality requirements. We envision that introducing a new metric (e.g., based on the gradient or connectivity error used in [348]) for SOD tasks, such as weighted F-measure [2] and S-measure [3], will be another important research direction.

(6) **Application Level:** The SOD task belongs to a more general task called class-agnostic object detection (CAOD). For simple scenes (e.g., those containing only one or two clear objects), SOD is identical to CAOD. From this point of view, SOD models have many potential applications in the real-world (e.g., Alibaba's fashion search system [339]), despite their currently limited number of representative cases [30], [31], [200].

## 8 CONCLUSION

In this survey, we identified and addressed the long-ignored *data selection bias* issue in SOD. Different from previous studies, we aimed to explore the SOD task in the wild. To achieve this goal, we collected a new challenging and densely annotated *SOC* dataset; analyzed a large number ( $\sim 200$ ) of representative models; conducted the most complete (top-100) benchmarking; devised a series of simple learning strategies to efficiently utilize negative samples and training data; and identified several current challenges and future directions. We hope that these contributions will provide the SOD community an opportunity to explore novel techniques in an open environment. We have tried to cover the most important works. Nevertheless, it is impractical to thoroughly investigate all models in this vast field. We will continue to incorporate new techniques on our website.

## REFERENCES

- [1] D.-P. Fan, M.-M. Cheng, J.-J. Liu, S.-H. Gao, Q. Hou, and A. Borji, "Salient objects in clutter: Bringing salient object detection to the foreground," in *Eur. Conf. Comput. Vis.*, 2018, pp. 186–202.
- [2] R. Margolin, L. Zelnik-Manor, and A. Tal, "How to evaluate foreground maps?" in *IEEE Conf. Comput. Vis. Pattern Recog.*, 2014, pp. 248–255.
- [3] D.-P. Fan, M.-M. Cheng, Y. Liu, T. Li, and A. Borji, "Structure-measure: A New Way to Evaluate Foreground Maps," in *Int. Conf. Comput. Vis.*, 2017, pp. 4548–4557.
- [4] D.-P. Fan, C. Gong, Y. Cao, B. Ren, M.-M. Cheng, and A. Borji, "Enhanced-alignment Measure for Binary Foreground Map Evaluation," in *Int. Joint Conf. Artif. Intell.*, 2018, pp. 698–704.
- [5] P. Zhang, T. Zhuo, W. Huang, K. Chen, and M. Kankanalli, "Online object tracking based on cnn with spatial-temporal saliency guided sampling," *Neurocomputing*, vol. 257, pp. 115–127, 2017.
- [6] A. Borji, S. Frintrop, D. N. Sihite, and L. Itti, "Adaptive object tracking by learning background context," in *IEEE Conf. Comput. Vis. Pattern Recog. Worksh.*, 2012, pp. 23–30.
- [7] V. Mahadevan and N. Vasconcelos, "On the connections between saliency and tracking," in *Adv. Neural Inform. Process. Syst.*, 2012, pp. 1664–1672.
- [8] A. Abdulmunem, Y.-K. Lai, and X. Sun, "Saliency guided local and global descriptors for effective action recognition," *Comput. Vis. Media*, vol. 2, no. 1, pp. 97–106, 2016.
- [9] J. He, J. Feng, X. Liu, T. Cheng, T.-H. Lin, H. Chung, and S.-F. Chang, "Mobile product search with bag of hash bits and boundary reranking," in *IEEE Conf. Comput. Vis. Pattern Recog.*, 2012, pp. 3005–3012.
- [10] G. Liu and D. Fan, "A model of visual attention for natural image retrieval," in *IEEE Int. Conf. Inf. Sci. Cloud Comput. Companion*, 2013, pp. 728–733.
- [11] J.-Y. Zhu, J. Wu, Y. Xu, E. Chang, and Z. Tu, "Unsupervised object class discovery via saliency-guided multiple class learning," *IEEE Trans. Pattern Anal. Mach. Intell.*, vol. 37, no. 4, pp. 862–875, 2015.
- [12] H. Liu, L. Zhang, and H. Huang, "Web-image driven best views of 3d shapes," *The Vis. Comput.*, vol. 28, no. 3, pp. 279–287, 2012.
- [13] K. Gu, G. Zhai, X. Yang, W. Zhang, and C. W. Chen, "Automatic contrast enhancement technology with saliency preservation," *IEEE Trans. Circ. Syst. Video Technol.*, vol. 25, no. 9, pp. 1480–1494, 2015.
- [14] R. Zhao, W. Ouyang, and X. Wang, "Unsupervised saliency learning for person re-identification," in *IEEE Conf. Comput. Vis. Pattern Recog.*, 2013, pp. 3586–3593.
- [15] M. Donoser, M. Urschler, M. Hirzer, and H. Bischof, "Saliency driven total variation segmentation," in *Int. Conf. Comput. Vis.*, 2009, pp. 817–824.
- [16] S. J. Oh, R. Benenson, A. Khoreva, Z. Akata, M. Fritz, and B. Schiele, "Exploiting saliency for object segmentation from image level labels," in *IEEE Conf. Comput. Vis. Pattern Recog.*, 2017, pp. 4410–4419.
- [17] D.-P. Fan, W. Wang, M.-M. Cheng, and J. Shen, "Shifting more attention to video salient object detection," in *IEEE Conf. Comput. Vis. Pattern Recog.*, 2019, pp. 8554–8564.
- [18] T. Chen, M.-M. Cheng, P. Tan, A. Shamir, and S.-M. Hu, "Sketch2photo: Internet image montage," *ACM Trans. Graph.*, vol. 28, no. 5, p. 124, 2009.
- [19] M.-M. Cheng, F.-L. Zhang, N. J. Mitra, X. Huang, and S.-M. Hu, "Repfinder: finding approximately repeated scene elements for image editing," *ACM Trans. Graph.*, vol. 29, no. 4, p. 83, 2010.
- [20] V. Ramanishka, A. Das, J. Zhang, and K. Saenko, "Top-down visual saliency guided by captions," in *IEEE Conf. Comput. Vis. Pattern Recog.*, vol. 1, no. 2, 2017, p. 7.
- [21] C. Guo and L. Zhang, "A novel multiresolution spatiotemporal saliency detection model and its applications in image and video compression," *IEEE Trans. Image Process.*, vol. 19, no. 1, pp. 185–198, 2010.
- [22] H. Hadizadeh and I. V. Bajic, "Saliency-aware video compression," *IEEE Trans. Image Process.*, vol. 23, no. 1, pp. 19–33, 2014.
- [23] Y. Liu, Z. Xu, W. Ye, Z. Zhang, S. Weng, C.-C. Chang, and H. Tang, "Image neural style transfer with preserving the salient regions," *IEEE Access*, vol. 7, pp. 40027–40037, 2019.
- [24] M.-M. Cheng, X.-C. Liu, J. Wang, S.-P. Lu, Y.-K. Lai, and P. L. Rosin, "Structure-preserving neural style transfer," *IEEE Trans. Image Process.*, vol. 29, pp. 909–920, 2020.
- [25] A. Toshev, J. Shi, and K. Daniilidis, "Image matching via saliency region correspondences," in *IEEE Conf. Comput. Vis. Pattern Recog.*, 2007, pp. 1–8.
- [26] M. J. Islam, R. Wang, K. de Langis, and J. Sattar, "Svam: Saliency-guided visual attention modeling by autonomous underwater robots," *arXiv preprint arXiv:2011.06252*, 2020.

- [27] D.-P. Fan, G.-P. Ji, G. Sun, M.-M. Cheng, J. Shen, and L. Shao, "Camouflaged object detection," in *IEEE Conf. Comput. Vis. Pattern Recog.*, 2020, pp. 2777–2787.
- [28] Y. Tu, L. Niu, W. Zhao, D. Cheng, and L. Zhang, "Image cropping with composition and saliency aware aesthetic score map," in *AAAI Conf. Art. Intell.*, vol. 34, no. 07, 2020, pp. 12 104–12 111.
- [29] J. Kim, T. Misu, Y.-T. Chen, A. Tawari, and J. Canny, "Grounding human-to-vehicle advice for self-driving vehicles," in *IEEE Conf. Comput. Vis. Pattern Recog.*, 2019, pp. 10 591–10 599.
- [30] N. Kumar, P. N. Belhumeur, A. Biswas, D. W. Jacobs, W. J. Kress, I. C. Lopez, and J. V. Soares, "Leafsnap: A computer vision system for automatic plant species identification," in *Eur. Conf. Comput. Vis.*, 2012, pp. 502–516.
- [31] X. Qin, D.-P. Fan, C. Huang, C. Diagne, Z. Zhang, A. C. Sant'Anna, A. Suárez, M. Jagersand, and L. Shao, "Boundary-aware segmentation network for mobile and web applications," *arXiv preprint arXiv:2101.04704*, 2021.
- [32] T. Liu, J. Sun, N. Zheng, X. Tang, and H.-Y. Shum, "Learning to detect a salient object," in *IEEE Conf. Comput. Vis. Pattern Recog.*, 2007, pp. 1–8.
- [33] S. Alpert, M. Galun, R. Basri, and A. Brandt, "Image segmentation by probabilistic bottom-up aggregation and cue integration," in *IEEE Conf. Comput. Vis. Pattern Recog.*, 2007, pp. 1–8.
- [34] D. Martin, C. Fowlkes, D. Tal, and J. Malik, "A database of human segmented natural images and its application to evaluating segmentation algorithms and measuring ecological statistics," in *Int. Conf. Comput. Vis.*, vol. 2, 2001, pp. 416–423.
- [35] M.-M. Cheng, N. J. Mitra, X. Huang, P. H. S. Torr, and S.-M. Hu, "Global contrast based salient region detection," *IEEE Trans. Pattern Anal. Mach. Intell.*, vol. 37, no. 3, pp. 569–582, 2015.
- [36] A. Borji, D. N. Sihite, and L. Itti, "Salient object detection: a benchmark," in *Eur. Conf. Comput. Vis.*, 2012, pp. 414–429.
- [37] Q. Yan, L. Xu, J. Shi, and J. Jia, "Hierarchical saliency detection," in *IEEE Conf. Comput. Vis. Pattern Recog.*, 2013, pp. 1155–1162.
- [38] C. Yang, L. Zhang, H. Lu, X. Ruan, and M.-H. Yang, "Saliency detection via graph-based manifold ranking," in *IEEE Conf. Comput. Vis. Pattern Recog.*, 2013, pp. 3166–3173.
- [39] Y. Li, X. Hou, C. Koch, J. M. Rehg, and A. L. Yuille, "The secrets of salient object segmentation," in *IEEE Conf. Comput. Vis. Pattern Recog.*, 2014, pp. 280–287.
- [40] G. Li and Y. Yu, "Visual saliency based on multiscale deep features," in *IEEE Conf. Comput. Vis. Pattern Recog.*, 2015, pp. 5455–5463.
- [41] L. Wang, H. Lu, Y. Wang, M. Feng, D. Wang, B. Yin, and X. Ruan, "Learning to detect salient objects with image-level supervision," in *IEEE Conf. Comput. Vis. Pattern Recog.*, 2017, pp. 136–145.
- [42] Z. Yang, S. Soltanian-Zadeh, and S. Farsiu, "Biconnet: An edge-preserved connectivity-based approach for salient object detection," *arXiv preprint arXiv:2103.00334*, 2021.
- [43] A. Torralba and A. A. Efros, "Unbiased look at dataset bias," in *IEEE Conf. Comput. Vis. Pattern Recog.*, 2011, pp. 1521–1528.
- [44] Z. Wu, L. Su, and Q. Huang, "Stacked cross refinement network for edge-aware salient object detection," in *IEEE Conf. Comput. Vis. Pattern Recog.*, 2019, pp. 7264–7273.
- [45] L. Itti, C. Koch, and E. Niebur, "A model of saliency-based visual attention for rapid scene analysis," *IEEE Trans. Pattern Anal. Mach. Intell.*, vol. 20, no. 11, pp. 1254–1259, 1998.
- [46] A. Borji, "Saliency prediction in the deep learning era: Successes and limitations," *IEEE Trans. Pattern Anal. Mach. Intell.*, vol. 43, no. 2, pp. 679–700, 2021.
- [47] T. Liu, J. Sun, N. Zheng, X. Tang, and H. Shum, "Learning to detect a salient object," in *IEEE Conf. Comput. Vis. Pattern Recog.*, 2007, pp. 1–8.
- [48] T. Liu, Z. Yuan, J. Sun, J. Wang, N. Zheng, X. Tang, and H.-Y. Shum, "Learning to detect a salient object," *IEEE Trans. Pattern Anal. Mach. Intell.*, vol. 33, no. 2, pp. 353–367, 2010.
- [49] P. Zhang, W. Liu, Y. Zeng, Y. Lei, and H. Lu, "Looking for the detail and context devils: High-resolution salient object detection," *IEEE Trans. Image Process.*, 2021.
- [50] Y. Zeng, P. Zhang, J. Zhang, Z. Lin, and H. Lu, "Towards high-resolution salient object detection," in *Int. Conf. Comput. Vis.*, 2019, pp. 7234–7243.
- [51] Q. Zhang, R. Cong, C. Li, M.-M. Cheng, Y. Fang, X. Cao, Y. Zhao, and S. Kwong, "Dense attention fluid network for salient object detection in optical remote sensing images," *IEEE Trans. Image Process.*, 2020.
- [52] M. Zhuge, D.-P. Fan, N. Liu, D. Zhang, D. Xu, and L. Shao, "Salient object detection via integrity learning," *arXiv preprint arXiv:2101.07663*, 2021.
- [53] Y. Zhou, S. Huo, W. Xiang, C. Hou, and S.-Y. Kung, "Semi-supervised salient object detection using a linear feedback control system model," *IEEE Trans. Cybern.*, vol. 49, no. 4, pp. 1173–1185, 2019.
- [54] G. Li, Y. Xie, and L. Lin, "Weakly supervised salient object detection using image labels," in *AAAI Conf. Art. Intell.*, vol. 32, no. 1, 2018.
- [55] L. Zhang, J. Zhang, Z. Lin, H. Lu, and Y. He, "Capsal: Leveraging captioning to boost semantics for salient object detection," in *IEEE Conf. Comput. Vis. Pattern Recog.*, 2019, pp. 6024–6033.
- [56] J. Zhang, X. Yu, A. Li, P. Song, B. Liu, and Y. Dai, "Weakly-supervised salient object detection via scribble annotations," in *IEEE Conf. Comput. Vis. Pattern Recog.*, 2020, pp. 12 546–12 555.
- [57] Y. Zeng, M. Feng, H. Lu, G. Yang, and A. Borji, "An unsupervised game-theoretic approach to saliency detection," *IEEE Trans. Image Process.*, vol. 27, no. 9, pp. 4545–4554, 2018.
- [58] J. Zhang, T. Zhang, Y. Dai, M. Harandi, and R. Hartley, "Deep unsupervised saliency detection: A multiple noisy labeling perspective," in *IEEE Conf. Comput. Vis. Pattern Recog.*, 2018, pp. 9029–9038.
- [59] T. Nguyen, M. Dax, C. K. Mummadi, N. Ngo, T. H. P. Nguyen, Z. Lou, and T. Brox, "Deepups: Deep robust unsupervised saliency prediction via self-supervision," in *Adv. Neural Inform. Process. Syst.*, vol. 32, 2019, pp. 204–214.
- [60] J. Wang, S. Zhu, J. Xu, and D. Cao, "The retrieval of the beautiful: Self-supervised salient object detection for beauty product retrieval," in *ACM Int. Conf. Multimedia*, 2019, pp. 2548–2552.
- [61] G. Li, Y. Xie, L. Lin, and Y. Yu, "Instance-level salient object segmentation," in *IEEE Conf. Comput. Vis. Pattern Recog.*, 2017, pp. 2386–2395.
- [62] R. Fan, M.-M. Cheng, Q. Hou, T.-J. Mu, J. Wang, and S.-M. Hu, "S4net: Single stage salient-instance segmentation," in *IEEE Conf. Comput. Vis. Pattern Recog.*, 2019, pp. 6103–6112.
- [63] J. Zhang, S. Ma, M. Sameki, S. Sclaroff, M. Betke, Z. Lin, X. Shen, B. Price, and R. Mech, "Salient object subitizing," in *IEEE Conf. Comput. Vis. Pattern Recog.*, 2015, pp. 4045–4054.
- [64] M. A. Islam, M. Kalash, and N. D. Bruce, "Revisiting salient object detection: Simultaneous detection, ranking, and subitizing of multiple salient objects," in *IEEE Conf. Comput. Vis. Pattern Recog.*, 2018, pp. 7142–7150.
- [65] S. He, J. Jiao, X. Zhang, G. Han, and R. W. Lau, "Delving into salient object subitizing and detection," in *IEEE Conf. Comput. Vis. Pattern Recog.*, 2017, pp. 1059–1067.
- [66] M. Kalash, M. A. Islam, and N. D. Bruce, "Relative saliency and ranking: Models, metrics, data and benchmarks," *IEEE Trans. Pattern Anal. Mach. Intell.*, vol. 43, no. 1, pp. 204–219, 2019.
- [67] A. Siris, J. Jiao, G. K. Tam, X. Xie, and R. W. Lau, "Inferring attention shift ranks of objects for image saliency," in *IEEE Conf. Comput. Vis. Pattern Recog.*, 2020, pp. 12 133–12 143.
- [68] A. Borji and L. Itti, "State-of-the-art in visual attention modeling," *IEEE Trans. Pattern Anal. Mach. Intell.*, vol. 35, no. 1, pp. 185–207, 2012.
- [69] A. Borji, M.-M. Cheng, H. Jiang, and J. Li, "Salient object detection: A benchmark," *IEEE Trans. Image Process.*, vol. 24, no. 12, pp. 5706–5722, 2015.
- [70] T. V. Nguyen, Q. Zhao, and S. Yan, "Attentive systems: A survey," *Int. J. Comput. Vis.*, vol. 126, no. 1, pp. 86–110, 2018.
- [71] A. Borji, M.-M. Cheng, Q. Hou, H. Jiang, and J. Li, "Salient object detection: A survey," *Comput. Vis. Media*, vol. 5, no. 2, pp. 117–150, 2019.
- [72] D. Zhang, H. Fu, J. Han, A. Borji, and X. Li, "A review of co-saliency detection algorithms: Fundamentals, applications, and challenges," *ACM Trans. Intell. Syst. Technol.*, vol. 9, no. 4, pp. 1–31, 2018.
- [73] R. Cong, J. Lei, H. Fu, M.-M. Cheng, W. Lin, and Q. Huang, "Review of visual saliency detection with comprehensive information," *IEEE Trans. Circ. Syst. Video Technol.*, vol. 29, no. 10, pp. 2941–2959, 2018.
- [74] J. Han, D. Zhang, G. Cheng, N. Liu, and D. Xu, "Advanced deep-learning techniques for salient and category-specific object detection: a survey," *IEEE Signal Process. Mag.*, vol. 35, no. 1, pp. 84–100, 2018.
- [75] A. Borji, "Saliency prediction in the deep learning era: An empirical investigation," *arXiv preprint arXiv:1810.03716*, vol. 10, 2018.
- [76] W. Wang, Q. Lai, H. Fu, J. Shen, H. Ling, and R. Yang, "Salient object detection in the deep learning era: An in-depth survey," *IEEE Trans. Pattern Anal. Mach. Intell.*, 2021.
- [77] D.-P. Fan, Z. Lin, Z. Zhang, M. Zhu, and M.-M. Cheng, "Rethinking rgb-d salient object detection: Models, data sets, and large-scale benchmarks," *IEEE T. Neural Netw. Learn. Syst.*, 2021.
- [78] T. Zhou, D.-P. Fan, M.-M. Cheng, J. Shen, and L. Shao, "Rgb-d salient object detection: A survey," *Comput. Vis. Media*, pp. 37–69, 2021.

- [79] Y. Jiang, T. Zhou, G.-P. Ji, K. Fu, Q. Zhao, and D.-P. Fan, "Light field salient object detection: A review and benchmark," *arXiv preprint arXiv:2010.04968*, 2020.
- [80] D.-P. Fan, T. Li, Z. Lin, G.-P. Ji, D. Zhang, M.-M. Cheng, H. Fu, and J. Shen, "Re-thinking co-salient object detection," *IEEE Trans. Pattern Anal. Mach. Intell.*, 2021.
- [81] J. Li, J. Su, C. Xia, and Y. Tian, "Distortion-adaptive salient object detection in 360° omnidirectional images," *IEEE J. Sel. Top. Signal. Process.*, vol. 14, no. 1, pp. 38–48, 2019.
- [82] R. Achanta, S. Hemami, F. Estrada, and S. Süsstrunk, "Frequency-tuned salient region detection," in *IEEE Conf. Comput. Vis. Pattern Recog.*, 2009, pp. 1597–1604.
- [83] V. Movahedi and J. H. Elder, "Design and perceptual validation of performance measures for salient object segmentation," in *IEEE Conf. Comput. Vis. Pattern Recog. Worksh.*, 2010, pp. 49–56.
- [84] M.-M. Cheng, G.-X. Zhang, N. J. Mitra, X. Huang, and S.-M. Hu, "Global contrast based salient region detection," in *IEEE Conf. Comput. Vis. Pattern Recog.*, 2011, pp. 409–416.
- [85] C. Xia, J. Li, X. Chen, A. Zheng, and Y. Zhang, "What is and what is not a salient object? learning salient object detector by ensembling linear exemplar regressors," in *IEEE Conf. Comput. Vis. Pattern Recog.*, 2017, pp. 4142–4150.
- [86] H. Jiang, M.-M. Cheng, S.-J. Li, A. Borji, and J. Wang, "Joint salient object detection and existence prediction," *Front. Comput. Sci.*, vol. 13, no. 4, pp. 778–788, 2019.
- [87] T.-Y. Lin, M. Maire, S. Belongie, J. Hays, P. Perona, D. Ramanan, P. Dollár, and C. L. Zitnick, "Microsoft COCO: Common objects in context," in *Eur. Conf. Comput. Vis.*, 2014, pp. 740–755.
- [88] P. Krähenbühl and V. Koltun, "Efficient inference in fully connected crfs with gaussian edge potentials," in *Adv. Neural Inform. Process. Syst.*, 2011.
- [89] Y. Boykov, O. Veksler, and R. Zabih, "Fast approximate energy minimization via graph cuts," *IEEE Trans. Pattern Anal. Mach. Intell.*, vol. 23, no. 11, pp. 1222–1239, 2001.
- [90] C. Rother, K. Vladimir, and B. Andrew, "Grabcut: interactive foreground extraction using iterated graph cuts," *ACM Trans. Graph.*, vol. 23, no. 3, pp. 309–314, 2004.
- [91] J. Shi and M. Jitendra, "Normalized cuts and image segmentation," *IEEE Trans. Pattern Anal. Mach. Intell.*, vol. 22, no. 8, pp. 888–905, 2000.
- [92] Y. Boykov and V. Kolmogorov, "An experimental comparison of min-cut/max-flow algorithms for energy minimization in vision," *IEEE Trans. Pattern Anal. Mach. Intell.*, vol. 26, no. 9, pp. 1124–1137, 2004.
- [93] J. Harel, C. Koch, and P. Perona, "Graph-based visual saliency," in *Adv. Neural Inform. Process. Syst.*, 2007, pp. 545–552.
- [94] X. Hou and L. Zhang, "Saliency detection: A spectral residual approach," in *IEEE Conf. Comput. Vis. Pattern Recog.*, 2007, pp. 1–8.
- [95] N. Bruce and J. Tsotsos, "Saliency based on information maximization," in *Adv. Neural Inform. Process. Syst.*, 2006, pp. 155–162.
- [96] L. Zhang, M. H. Tong, T. K. Marks, H. Shan, and G. W. Cottrell, "SUN: A Bayesian framework for saliency using natural statistics," *J. Vis.*, vol. 8, no. 7, pp. 32–32, 2008.
- [97] Y.-F. Ma and H.-J. Zhang, "Contrast-based image attention analysis by using fuzzy growing," in *ACM Int. Conf. Multimedia*, 2003, pp. 374–381.
- [98] R. Achanta, F. Estrada, P. Wils, and S. Süsstrunk, "Salient region detection and segmentation," in *Int. Conf. Comput. Vis. Syst.*, 2008, pp. 66–75.
- [99] E. Rahtu, J. Kannala, M. Salo, and J. Heikkilä, "Segmenting salient objects from images and videos," in *Eur. Conf. Comput. Vis.*, 2010, pp. 366–379.
- [100] R. Achanta and S. Süsstrunk, "Saliency detection using maximum symmetric surround," in *IEEE Int. Conf. Image Process.*, 2010, pp. 2653–2656.
- [101] R. Valenti, N. Sebe, T. Gevers *et al.*, "Image saliency by isocentric curvedness and color," in *Int. Conf. Comput. Vis.*, vol. 1, no. 3, 2009, p. 6.
- [102] P. L. Rosin, "A simple method for detecting salient regions," *Pattern Recogn.*, vol. 42, no. 11, pp. 2363–2371, 2009.
- [103] F. Liu and M. Gleicher, "Region enhanced scale-invariant saliency detection," in *Int. Conf. Multimedia and Expo*, 2006, pp. 1477–1480.
- [104] Y. Hu, D. Rajan, and L.-T. Chia, "Robust subspace analysis for detecting visual attention regions in images," in *ACM Int. Conf. Multimedia*, 2005, pp. 716–724.
- [105] Z. Yu and H.-S. Wong, "A rule based technique for extraction of visual attention regions based on real-time clustering," *IEEE Trans. Multimedia*, vol. 9, no. 4, pp. 766–784, 2007.
- [106] H. Yu, J. Li, Y. Tian, and T. Huang, "Automatic interesting object extraction from images using complementary saliency maps," in *ACM Int. Conf. Multimedia*, 2010, pp. 891–894.
- [107] Y. Xie, H. Lu, and M.-H. Yang, "Bayesian saliency via low and mid level cues," *IEEE Trans. Image Process.*, vol. 22, no. 5, pp. 1689–1698, 2012.
- [108] E. Erdem and A. Erdem, "Visual saliency estimation by nonlinearly integrating features using region covariances," *J. Vis.*, vol. 13, no. 4, pp. 11–11, 2013.
- [109] C. Yang, L. Zhang, and H. Lu, "Graph-regularized saliency detection with convex-hull-based center prior," *IEEE Signal Process. Lett.*, vol. 20, no. 7, pp. 637–640, 2013.
- [110] N. Tong, H. Lu, L. Zhang, and X. Ruan, "Saliency detection with multi-scale superpixels," *IEEE Signal Process. Lett.*, vol. 21, no. 9, pp. 1035–1039, 2014.
- [111] H. Peng, B. Li, R. Ji, W. Hu, W. Xiong, and C. Lang, "Salient object detection via low-rank and structured sparse matrix decomposition," in *AAAI Conf. Art. Intell.*, 2013.
- [112] J. Sun, H. Lu, and S. Li, "Saliency detection based on integration of boundary and soft-segmentation," in *IEEE Int. Conf. Image Process.*, 2012, pp. 1085–1088.
- [113] F. Perazzi, P. Krähenbühl, Y. Pritch, and A. Hornung, "Saliency filters: Contrast based filtering for salient region detection," in *IEEE Conf. Comput. Vis. Pattern Recog.*, 2012, pp. 733–740.
- [114] H. Jiang, J. Wang, Z. Yuan, Y. Wu, N. Zheng, and S. Li, "Salient object detection: A discriminative regional feature integration approach," in *IEEE Conf. Comput. Vis. Pattern Recog.*, 2013, pp. 2083–2090.
- [115] W. Zhu, S. Liang, Y. Wei, and J. Sun, "Saliency optimization from robust background detection," in *IEEE Conf. Comput. Vis. Pattern Recog.*, 2014, pp. 2814–2821.
- [116] X. Shen and Y. Wu, "A unified approach to salient object detection via low rank matrix recovery," in *IEEE Conf. Comput. Vis. Pattern Recog.*, 2012, pp. 853–860.
- [117] R. Margolin, A. Tal, and L. Zelnik-Manor, "What makes a patch distinct?" in *IEEE Conf. Comput. Vis. Pattern Recog.*, 2013, pp. 1139–1146.
- [118] J. Kim, D. Han, Y.-W. Tai, and J. Kim, "Salient region detection via high-dimensional color transform," in *IEEE Conf. Comput. Vis. Pattern Recog.*, 2014, pp. 883–890.
- [119] L. Mai, Y. Niu, and F. Liu, "Saliency aggregation: A data-driven approach," in *IEEE Conf. Comput. Vis. Pattern Recog.*, 2013, pp. 1131–1138.
- [120] C. Scharfenberger, A. Wong, K. Fergani, J. S. Zelek, and D. A. Clausi, "Statistical textural distinctiveness for salient region detection in natural images," in *IEEE Conf. Comput. Vis. Pattern Recog.*, 2013, pp. 979–986.
- [121] R. Liu, J. Cao, Z. Lin, and S. Shan, "Adaptive partial differential equation learning for visual saliency detection," in *IEEE Conf. Comput. Vis. Pattern Recog.*, 2014, pp. 3866–3873.
- [122] Z. Jiang and L. S. Davis, "Submodular salient region detection," in *IEEE Conf. Comput. Vis. Pattern Recog.*, 2013, pp. 2043–2050.
- [123] K. Shi, K. Wang, J. Lu, and L. Lin, "PISA: Pixelwise image saliency by aggregating complementary appearance contrast measures with spatial priors," in *IEEE Conf. Comput. Vis. Pattern Recog.*, 2013, pp. 2115–2122.
- [124] X. Li, H. Lu, L. Zhang, X. Ruan, and M.-H. Yang, "Saliency detection via dense and sparse reconstruction," in *Int. Conf. Comput. Vis.*, 2013, pp. 2976–2983.
- [125] B. Jiang, L. Zhang, H. Lu, C. Yang, and M.-H. Yang, "Saliency detection via absorbing markov chain," in *Int. Conf. Comput. Vis.*, 2013, pp. 1665–1672.
- [126] M.-M. Cheng, J. Warrell, W.-Y. Lin, S. Zheng, V. Vineet, and N. Crook, "Efficient salient region detection with soft image abstraction," in *Int. Conf. Comput. Vis.*, 2013, pp. 1529–1536.
- [127] K.-Y. Chang, T.-L. Liu, H.-T. Chen, and S.-H. Lai, "Fusing generic objectness and visual saliency for salient object detection," in *Int. Conf. Comput. Vis.*, 2011, pp. 914–921.
- [128] D. A. Klein and S. Frintrop, "Center-surround divergence of feature statistics for salient object detection," in *Int. Conf. Comput. Vis.*, 2011, pp. 2214–2219.
- [129] P. Jiang, H. Ling, J. Yu, and J. Peng, "Salient region detection by ufo: Uniqueness, focusness and objectness," in *Int. Conf. Comput. Vis.*, 2013, pp. 1976–1983.
- [130] X. Li, Y. Li, C. Shen, A. Dick, and A. Van Den Hengel, "Contextual hypergraph modeling for salient object detection," in *Int. Conf. Comput. Vis.*, 2013, pp. 3328–3335.
- [131] Y. Jia and M. Han, "Category-independent object-level saliency detection," in *Int. Conf. Comput. Vis.*, 2013, pp. 1761–1768.
- [132] Y. Lu, W. Zhang, H. Lu, and X. Xue, "Salient object detection using concavity context," in *Int. Conf. Comput. Vis.*, 2011, pp. 233–240.

- [133] Y. Wei, F. Wen, W. Zhu, and J. Sun, "Geodesic saliency using background priors," in *Eur. Conf. Comput. Vis.*, 2012, pp. 29–42.
- [134] H. Jiang, J. Wang, Z. Yuan, T. Liu, N. Zheng, and S. Li, "Automatic salient object segmentation based on context and shape prior," in *Brit. Mach. Vis. Conf.*, vol. 6, no. 7, 2011, p. 9.
- [135] W. Zou, K. Kpalma, Z. Liu, and J. Ronsin, "Segmentation driven low-rank matrix recovery for saliency detection," in *Brit. Mach. Vis. Conf.*, 2013, pp. 1–13.
- [136] H. Peng, B. Li, H. Ling, W. Hu, W. Xiong, and S. J. Maybank, "Salient object detection via structured matrix decomposition," *IEEE Trans. Pattern Anal. Mach. Intell.*, vol. 39, no. 4, pp. 818–832, 2016.
- [137] L. Zhang, C. Yang, H. Lu, X. Ruan, and M.-H. Yang, "Ranking saliency," *IEEE Trans. Pattern Anal. Mach. Intell.*, vol. 39, no. 9, pp. 1892–1904, 2017.
- [138] J. Wang, H. Lu, X. Li, N. Tong, and W. Liu, "Saliency detection via background and foreground seed selection," *Neurocomputing*, vol. 152, pp. 359–368, 2015.
- [139] N. Tong, H. Lu, Y. Zhang, and X. Ruan, "Salient object detection via global and local cues," *Pattern Recogn.*, vol. 48, no. 10, pp. 3258–3267, 2015.
- [140] S. Chen, L. Zheng, X. Hu, and P. Zhou, "Discriminative saliency propagation with sink points," *Pattern Recogn.*, vol. 60, pp. 2–12, 2016.
- [141] H. Li, H. Lu, Z. Lin, X. Shen, and B. Price, "Inner and inter label propagation: salient object detection in the wild," *IEEE Trans. Image Process.*, vol. 24, no. 10, pp. 3176–3186, 2015.
- [142] J. Sun, H. Lu, and X. Liu, "Saliency region detection based on markov absorption probabilities," *IEEE Trans. Image Process.*, vol. 24, no. 5, pp. 1639–1649, 2015.
- [143] F. Huang, J. Qi, H. Lu, L. Zhang, and X. Ruan, "Salient object detection via multiple instance learning," *IEEE Trans. Image Process.*, vol. 26, no. 4, pp. 1911–1922, 2017.
- [144] Y. Yuan, C. Li, J. Kim, W. Cai, and D. D. Feng, "Reversion correction and regularized random walk ranking for saliency detection," *IEEE Trans. Image Process.*, vol. 27, no. 3, pp. 1311–1322, 2017.
- [145] G.-H. Liu and J.-Y. Yang, "Exploiting color volume and color difference for salient region detection," *IEEE Trans. Image Process.*, vol. 28, no. 1, pp. 6–16, 2019.
- [146] K. Fu, C. Gong, I. Y.-H. Gu, and J. Yang, "Normalized cut-based saliency detection by adaptive multi-level region merging," *IEEE Trans. Image Process.*, vol. 24, no. 12, pp. 5671–5683, 2015.
- [147] X. Huang and Y.-J. Zhang, "300-fps salient object detection via minimum directional contrast," *IEEE Trans. Image Process.*, vol. 26, no. 9, pp. 4243–4254, 2017.
- [148] Q. Liu, X. Hong, B. Zou, J. Chen, Z. Chen, and G. Zhao, "Hierarchical contour closure-based holistic salient object detection," *IEEE Trans. Image Process.*, vol. 26, no. 9, pp. 4537–4552, 2017.
- [149] Y. Kong, J. Zhang, H. Lu, and X. Liu, "Exemplar-aided salient object detection via joint latent space embedding," *IEEE Trans. Image Process.*, vol. 27, no. 10, pp. 5167–5177, 2018.
- [150] S. Huo, Y. Zhou, J. Lei, N. Ling, and C. Hou, "Iterative feedback control-based salient object segmentation," *IEEE Trans. Multimedia*, vol. 20, no. 6, pp. 1350–1364, 2017.
- [151] S. Huo, Y. Zhou, W. Xiang, and S.-Y. Kung, "Semisupervised learning based on a novel iterative optimization model for saliency detection," *IEEE T. Neural Netw. Learn. Syst.*, vol. 30, no. 1, pp. 225–241, 2019.
- [152] J. Zhang, S. Sclaroff, Z. Lin, X. Shen, B. Price, and R. Mech, "Minimum barrier salient object detection at 80 fps," in *Int. Conf. Comput. Vis.*, 2015, pp. 1404–1412.
- [153] P. Jiang, N. Vasconcelos, and J. Peng, "Generic promotion of diffusion-based salient object detection," in *Int. Conf. Comput. Vis.*, 2015, pp. 217–225.
- [154] Y. Qin, H. Lu, Y. Xu, and H. Wang, "Saliency detection via cellular automata," in *IEEE Conf. Comput. Vis. Pattern Recog.*, 2015, pp. 110–119.
- [155] N. Otsu, "A threshold selection method from gray-level histograms," *IEEE Trans. Syst. Man Cybern. Syst.*, vol. 9, no. 1, pp. 62–66, 1979.
- [156] N. Tong, H. Lu, X. Ruan, and M.-H. Yang, "Salient object detection via bootstrap learning," in *IEEE Conf. Comput. Vis. Pattern Recog.*, 2015, pp. 1884–1892.
- [157] F. Yang, H. Lu, and Y.-W. Chen, "Human tracking by multiple kernel boosting with locality affinity constraints," in *Asian Conf. Comput. Vis.*, 2010, pp. 39–50.
- [158] W.-C. Tu, S. He, Q. Yang, and S.-Y. Chien, "Real-time salient object detection with a minimum spanning tree," in *IEEE Conf. Comput. Vis. Pattern Recog.*, 2016, pp. 2334–2342.
- [159] C. Li, Y. Yuan, W. Cai, Y. Xia, and D. Dagan Feng, "Robust saliency detection via regularized random walks ranking," in *IEEE Conf. Comput. Vis. Pattern Recog.*, 2015, pp. 2710–2717.
- [160] C. Gong, D. Tao, W. Liu, S. J. Maybank, M. Fang, K. Fu, and J. Yang, "Saliency propagation from simple to difficult," in *IEEE Conf. Comput. Vis. Pattern Recog.*, 2015, pp. 2531–2539.
- [161] N. Li, B. Sun, and J. Yu, "A weighted sparse coding framework for saliency detection," in *IEEE Conf. Comput. Vis. Pattern Recog.*, 2015, pp. 5216–5223.
- [162] Y. Kong, L. Wang, X. Liu, H. Lu, and X. Ruan, "Pattern mining saliency," in *Eur. Conf. Comput. Vis.*, 2016, pp. 583–598.
- [163] Y. Liu, J. Han, Q. Zhang, and L. Wang, "Salient object detection via two-stage graphs," *IEEE Trans. Circ. Syst. Video Technol.*, vol. 29, no. 4, pp. 1023–1037, 2019.
- [164] Y. Zhou, T. Zhang, S. Huo, C. Hou, and S.-Y. Kung, "Adaptive irregular graph construction-based salient object detection," *IEEE Trans. Circ. Syst. Video Technol.*, vol. 30, no. 6, pp. 1569–1582, 2020.
- [165] Y. Zhou, A. Mao, S. Huo, J. Lei, and S.-Y. Kung, "Salient object detection via fuzzy theory and object-level enhancement," *IEEE Trans. Multimedia*, vol. 21, no. 1, pp. 74–85, 2019.
- [166] X. Lin, Z.-J. Wang, L. Ma, and X. Wu, "Saliency detection via multi-scale global cues," *IEEE Trans. Multimedia*, vol. 21, no. 7, pp. 1646–1659, 2019.
- [167] Y. Xu, X. Hong, F. Porikli, X. Liu, J. Chen, and G. Zhao, "Saliency integration: An arbitrator model," *IEEE Trans. Multimedia*, vol. 21, no. 1, pp. 98–113, 2019.
- [168] N. Liu and J. Han, "Dhsnet: Deep hierarchical saliency network for salient object detection," in *IEEE Conf. Comput. Vis. Pattern Recog.*, 2016, pp. 678–686.
- [169] L. Zhang, J. Sun, T. Wang, Y. Min, and H. Lu, "Visual saliency detection via kernelized subspace ranking with active learning," *IEEE Trans. Image Process.*, vol. 29, pp. 2258–2270, 2020.
- [170] X. Huang, Y. Zheng, J. Huang, and Y.-J. Zhang, "50 fps object-level saliency detection via maximally stable region," *IEEE Trans. Image Process.*, vol. 29, pp. 1384–1396, 2020.
- [171] R. Strand, K. C. Ciesielski, F. Malmberg, and P. K. Saha, "The minimum barrier distance," *Comput. Vis. Image Underst.*, vol. 117, no. 4, pp. 429–437, 2013.
- [172] Y.-Y. Zhang, S. Zhang, P. Zhang, H.-Z. Song, and X.-G. Zhang, "Local regression ranking for saliency detection," *IEEE Trans. Image Process.*, vol. 29, pp. 1536–1547, 2020.
- [173] M. Everingham, L. Van Gool, C. Williams, J. Winn, and A. Zisserman, "The pascal visual object classes challenge 2012 (voc2012) results (2012)," in URL <http://www.pascal-network.org/challenges/VOC/voc2011/workshop/index.html>, 2011.
- [174] S. He, R. W. Lau, W. Liu, Z. Huang, and Q. Yang, "Supercnn: A superpixelwise convolutional neural network for salient object detection," *Int. J. Comput. Vis.*, vol. 115, no. 3, pp. 330–344, 2015.
- [175] L. Wang, H. Lu, X. Ruan, and M.-H. Yang, "Deep networks for saliency detection via local estimation and global search," in *IEEE Conf. Comput. Vis. Pattern Recog.*, 2015, pp. 3183–3192.
- [176] R. Zhao, W. Ouyang, H. Li, and X. Wang, "Saliency detection by multi-context deep learning," in *IEEE Conf. Comput. Vis. Pattern Recog.*, 2015, pp. 1265–1274.
- [177] C. Szegedy, W. Liu, Y. Jia, P. Sermanet, S. Reed, D. Anguelov, D. Erhan, V. Vanhoucke, and A. Rabinovich, "Going deeper with convolutions," in *IEEE Conf. Comput. Vis. Pattern Recog.*, 2015, pp. 1–9.
- [178] Y. Yuan, C. Li, J. Kim, W. Cai, and D. D. Feng, "Dense and sparse labeling with multidimensional features for saliency detection," *IEEE Trans. Circ. Syst. Video Technol.*, vol. 28, no. 5, pp. 1130–1143, 2016.
- [179] Y. LeCun, L. Bottou, Y. Bengio, and P. Haffner, "Gradient-based learning applied to document recognition," *IEEE Inst. Electr. Electron. Eng.*, vol. 86, no. 11, pp. 2278–2324, 1998.
- [180] T. Chen, L. Lin, L. Liu, X. Luo, and X. Li, "DISC: Deep image saliency computing via progressive representation learning," *IEEE T. Neural Netw. Learn. Syst.*, vol. 27, no. 6, pp. 1135–1149, 2016.
- [181] X. Li, L. Zhao, L. Wei, M.-H. Yang, F. Wu, Y. Zhuang, H. Ling, and J. Wang, "Deepsaliency: Multi-task deep neural network model for salient object detection," *IEEE Trans. Image Process.*, vol. 25, no. 8, pp. 3919–3930, 2016.
- [182] K. Simonyan and A. Zisserman, "Very deep convolutional networks for large-scale image recognition," in *Int. Conf. Learn. Represent.*, 2015.
- [183] J. Kim and V. Pavlovic, "A shape-based approach for salient object detection using deep learning," in *Eur. Conf. Comput. Vis.*, 2016, pp. 455–470.

- [184] A. Krizhevsky, S. Ilya, and G. E Hinton, "Imagenet classification with deep convolutional neural networks," in *Adv. Neural Inform. Process. Syst.*, 2012.
- [185] Y. Tang and X. Wu, "Saliency detection via combining region-level and pixel-level predictions with cnns," in *Eur. Conf. Comput. Vis.*, 2016, pp. 809–825.
- [186] L. Wang, L. Wang, H. Lu, P. Zhang, and X. Ruan, "Saliency detection with recurrent fully convolutional networks," in *Eur. Conf. Comput. Vis.*, 2016, pp. 825–841.
- [187] J. Zhang, S. Sclaroff, Z. Lin, X. Shen, B. Price, and R. Mech, "Unconstrained salient object detection via proposal subset optimization," in *IEEE Conf. Comput. Vis. Pattern Recog.*, 2016, pp. 5733–5742.
- [188] S. S. Kruthiventi, V. Gudisa, J. H. Dholakiya, and R. Venkatesh Babu, "Saliency unified: A deep architecture for simultaneous eye fixation prediction and salient object segmentation," in *IEEE Conf. Comput. Vis. Pattern Recog.*, 2016, pp. 5781–5790.
- [189] M. Jiang, S. Huang, J. Duan, and Q. Zhao, "SALICON: Saliency in context," in *IEEE Conf. Comput. Vis. Pattern Recog.*, 2015, pp. 1072–1080.
- [190] J. Kuen, Z. Wang, and G. Wang, "Recurrent attentional networks for saliency detection," in *IEEE Conf. Comput. Vis. Pattern Recog.*, 2016, pp. 3668–3677.
- [191] R. Ju, L. Ge, W. Geng, T. Ren, and G. Wu, "Depth saliency based on anisotropic center-surround difference," in *IEEE Int. Conf. Image Process.*, 2014, pp. 1115–1119.
- [192] H. Peng, B. Li, W. Xiong, W. Hu, and R. Ji, "Rgbd salient object detection: a benchmark and algorithms," in *Eur. Conf. Comput. Vis.*, 2014, pp. 92–109.
- [193] G. Lee, Y.-W. Tai, and J. Kim, "Deep saliency with encoded low level distance map and high level features," in *IEEE Conf. Comput. Vis. Pattern Recog.*, 2016, pp. 660–668.
- [194] G. Li and Y. Yu, "Deep contrast learning for salient object detection," in *IEEE Conf. Comput. Vis. Pattern Recog.*, 2016, pp. 478–487.
- [195] P. Hu, B. Shuai, J. Liu, and G. Wang, "Deep level sets for salient object detection," in *IEEE Conf. Comput. Vis. Pattern Recog.*, 2017, pp. 2300–2309.
- [196] T. Wang, A. Borji, L. Zhang, P. Zhang, and H. Lu, "A stagewise refinement model for detecting salient objects in images," in *IEEE Conf. Comput. Vis. Pattern Recog.*, 2017, pp. 4019–4028.
- [197] K. He, X. Zhang, S. Ren, and J. Sun, "Deep residual learning for image recognition," in *IEEE Conf. Comput. Vis. Pattern Recog.*, 2016, pp. 770–778.
- [198] Z. Luo, A. Mishra, A. Achkar, J. Eichel, S. Li, and P.-M. Jodoin, "Non-local deep features for salient object detection," in *IEEE Conf. Comput. Vis. Pattern Recog.*, 2017, pp. 6609–6617.
- [199] J. Deng, W. Dong, R. Socher, L.-J. Li, K. Li, and L. Fei-Fei, "Imagenet: A large-scale hierarchical image database," in *IEEE Conf. Comput. Vis. Pattern Recog.*, 2009, pp. 248–255.
- [200] Q. Hou, M.-M. Cheng, X. Hu, A. Borji, Z. Tu, and P. H. Torr, "Deeply supervised salient object detection with short connections," in *IEEE Conf. Comput. Vis. Pattern Recog.*, 2017, pp. 3203–3212.
- [201] X. Chen, A. Zheng, J. Li, and F. Lu, "Look, perceive and segment: Finding the salient objects in images via two-stream fixation-semantic cnns," in *Int. Conf. Comput. Vis.*, 2017, pp. 1050–1058.
- [202] D. Zhang, J. Han, and Y. Zhang, "Supervision by fusion: Towards unsupervised learning of deep salient object detector," in *Int. Conf. Comput. Vis.*, 2017, pp. 4048–4056.
- [203] P. Zhang, D. Wang, H. Lu, H. Wang, and B. Yin, "Learning uncertain convolutional features for accurate saliency detection," in *Int. Conf. Comput. Vis.*, 2017, pp. 212–221.
- [204] P. Zhang, D. Wang, H. Lu, H. Wang, and X. Ruan, "Amulet: Aggregating multi-level convolutional features for salient object detection," in *Int. Conf. Comput. Vis.*, 2017, pp. 202–211.
- [205] S. Chen, B. Wang, X. Tan, and X. Hu, "Embedding attention and residual network for accurate salient object detection," *IEEE Trans. Cybern.*, 2018.
- [206] K. Fu, Q. Zhao, and I. Y.-H. Gu, "Refinet: A deep segmentation assisted refinement network for salient object detection," *IEEE Trans. Multimedia*, vol. 21, no. 2, pp. 457–469, 2018.
- [207] C. Cao, Y. Huang, Z. Wang, L. Wang, N. Xu, and T. Tan, "Lateral inhibition-inspired convolutional neural network for visual attention and saliency detection," in *AAAI Conf. Art. Intell.*, 2018.
- [208] X. Hu, L. Zhu, J. Qin, C.-W. Fu, and P.-A. Heng, "Recurrently aggregating deep features for salient object detection," in *AAAI Conf. Art. Intell.*, 2018.
- [209] Z. Deng, X. Hu, L. Zhu, X. Xu, J. Qin, G. Han, and P.-A. Heng, "R3net: Recurrent residual refinement network for saliency detection," in *AAAI Conf. Art. Intell.*, 2018, pp. 684–690.
- [210] S. Xie, R. Girshick, P. Dollár, Z. Tu, and K. He, "Aggregated residual transformations for deep neural networks," in *IEEE Conf. Comput. Vis. Pattern Recog.*, 2017, pp. 1492–1500.
- [211] X. Li, F. Yang, H. Cheng, W. Liu, and D. Shen, "Contour knowledge transfer for salient object detection," in *Eur. Conf. Comput. Vis.*, 2018, pp. 355–370.
- [212] S. Chen, X. Tan, B. Wang, and X. Hu, "Reverse attention for salient object detection," in *Eur. Conf. Comput. Vis.*, 2018, pp. 234–250.
- [213] Y. Zeng, H. Lu, L. Zhang, M. Feng, and A. Borji, "Learning to promote saliency detectors," in *IEEE Conf. Comput. Vis. Pattern Recog.*, 2018, pp. 1644–1653.
- [214] M. Amirul Islam, M. Kalash, and N. D. Bruce, "Revisiting salient object detection: Simultaneous detection, ranking, and subitizing of multiple salient objects," in *IEEE Conf. Comput. Vis. Pattern Recog.*, 2018, pp. 7142–7150.
- [215] W. Wang, J. Shen, X. Dong, and A. Borji, "Salient object detection driven by fixation prediction," in *IEEE Conf. Comput. Vis. Pattern Recog.*, 2018, pp. 1711–1720.
- [216] L. Zhang, J. Dai, H. Lu, Y. He, and G. Wang, "A bi-directional message passing model for salient object detection," in *IEEE Conf. Comput. Vis. Pattern Recog.*, 2018, pp. 1741–1750.
- [217] T. Wang, L. Zhang, S. Wang, H. Lu, G. Yang, X. Ruan, and A. Borji, "Detect globally, refine locally: A novel approach to saliency detection," in *IEEE Conf. Comput. Vis. Pattern Recog.*, 2018, pp. 3127–3135.
- [218] N. Liu, J. Han, and M.-H. Yang, "Picanet: Learning pixel-wise contextual attention for saliency detection," in *IEEE Conf. Comput. Vis. Pattern Recog.*, 2018, pp. 3089–3098.
- [219] X. Zhang, T. Wang, J. Qi, H. Lu, and G. Wang, "Progressive attention guided recurrent network for salient object detection," in *IEEE Conf. Comput. Vis. Pattern Recog.*, 2018, pp. 714–722.
- [220] S. Zhou, J. Wang, F. Wang, and D. Huang, "Se2net: Siamese edge-enhancement network for salient object detection," *arXiv preprint arXiv:1904.00048*, 2019.
- [221] Z. Li, C. Lang, Y. Chen, J. Liew, and J. Feng, "Deep reasoning with multi-scale context for salient object detection," *arXiv preprint arXiv:1901.08362*, 2019.
- [222] S. Jia and N. D. Bruce, "Richer and deeper supervision network for salient object detection," *arXiv preprint arXiv:1901.02425*, 2019.
- [223] L. Zhu, J. Chen, X. Hu, C.-W. Fu, X. Xu, J. Qin, and P.-A. Heng, "Aggregating attentional dilated features for salient object detection," *IEEE Trans. Circ. Syst. Video Technol.*, vol. 30, no. 10, pp. 3358–3371, 2019.
- [224] G. Huang, Z. Liu, L. Van Der Maaten, and K. Q. Weinberger, "Densely connected convolutional networks," in *IEEE Conf. Comput. Vis. Pattern Recog.*, 2017, pp. 4700–4708.
- [225] Y. Tang and X. Wu, "Salient object detection using cascaded convolutional neural networks and adversarial learning," *IEEE Trans. Multimedia*, vol. 21, no. 9, pp. 2237–2247, 2019.
- [226] L.-C. Chen, G. Papandreou, I. Kokkinos, K. Murphy, and A. L. Yuille, "DeepLab: Semantic image segmentation with deep convolutional nets, atrous convolution, and fully connected crfs," *IEEE Trans. Pattern Anal. Mach. Intell.*, vol. 40, no. 4, pp. 834–848, 2018.
- [227] Y. Wang, X. Zhao, X. Hu, Y. Li, and K. Huang, "Focal boundary guided salient object detection," *IEEE Trans. Image Process.*, vol. 28, no. 6, pp. 2813–2824, 2019.
- [228] T. V. Nguyen, K. Nguyen, and T.-T. Do, "Semantic prior analysis for salient object detection?" *IEEE Trans. Image Process.*, vol. 28, no. 6, pp. 3130–3141, 2019.
- [229] M. Kampffmeyer, N. Dong, X. Liang, Y. Zhang, and E. P. Xing, "Connnet: A long-range relation-aware pixel-connectivity network for salient segmentation," *IEEE Trans. Image Process.*, vol. 28, no. 5, pp. 2518–2529, 2019.
- [230] P. Zhang, W. Liu, H. Lu, and C. Shen, "Salient object detection with lossless feature reflection and weighted structural loss," *IEEE Trans. Image Process.*, vol. 28, no. 6, pp. 3048–3060, 2019.
- [231] D. Zhang, J. Han, Y. Zhang, and D. Xu, "Synthesizing supervision for learning deep saliency network without human annotation," *IEEE Trans. Pattern Anal. Mach. Intell.*, vol. 42, no. 7, pp. 1755–1769, 2019.
- [232] C. Li, R. Cong, J. Hou, S. Zhang, Y. Qian, and S. Kwong, "Nested network with two-stream pyramid for salient object detection in optical remote sensing images," *IEEE Trans. Geosci. Remote. Sens.*, vol. 57, no. 11, pp. 9156–9166, 2019.

- [233] K. Fu, Q. Zhao, I. Y.-H. Gu, and J. Yang, "Deepside: A general deep framework for salient object detection," *Neurocomputing*, vol. 356, pp. 69–82, 2019.
- [234] B. Li, Z. Sun, and Y. Guo, "Supervae: Superpixelwise variational autoencoder for salient object detection," in *AAAI Conf. Art. Intell.*, vol. 33, no. 01, 2019, pp. 8569–8576.
- [235] Y. Zhuge, Y. Zeng, and H. Lu, "Deep embedding features for salient object detection," in *AAAI Conf. Art. Intell.*, 2019.
- [236] Y. Zeng, Y. Zhuge, H. Lu, L. Zhang, M. Qian, and Y. Yu, "Multi-source weak supervision for saliency detection," in *IEEE Conf. Comput. Vis. Pattern Recog.*, 2019, pp. 6074–6083.
- [237] R. Wu, M. Feng, W. Guan, D. Wang, H. Lu, and E. Ding, "A mutual learning method for salient object detection with intertwined multi-supervision," in *IEEE Conf. Comput. Vis. Pattern Recog.*, 2019, pp. 8150–8159.
- [238] W. Wang, J. Shen, M.-M. Cheng, and L. Shao, "An iterative and cooperative top-down and bottom-up inference network for salient object detection," in *IEEE Conf. Comput. Vis. Pattern Recog.*, 2019, pp. 5968–5977.
- [239] M. Feng, H. Lu, and E. Ding, "Attentive feedback network for boundary-aware salient object detection," in *IEEE Conf. Comput. Vis. Pattern Recog.*, 2019, pp. 1623–1632.
- [240] T. Zhao and X. Wu, "Pyramid feature attention network for saliency detection," in *IEEE Conf. Comput. Vis. Pattern Recog.*, 2019, pp. 3085–3094.
- [241] W. Wang, S. Zhao, J. Shen, S. C. Hoi, and A. Borji, "Salient object detection with pyramid attention and salient edges," in *IEEE Conf. Comput. Vis. Pattern Recog.*, 2019, pp. 1448–1457.
- [242] Z. Wu, L. Su, and Q. Huang, "Cascaded partial decoder for fast and accurate salient object detection," in *IEEE Conf. Comput. Vis. Pattern Recog.*, 2019, pp. 3907–3916.
- [243] J.-J. Liu, Q. Hou, M.-M. Cheng, J. Feng, and J. Jiang, "A simple pooling-based design for real-time salient object detection," in *IEEE Conf. Comput. Vis. Pattern Recog.*, 2019, pp. 3917–3926.
- [244] X. Qin, Z. Zhang, C. Huang, C. Gao, M. Dehghan, and M. Jagersand, "BASNet: Boundary-Aware Salient Object Detection," in *IEEE Conf. Comput. Vis. Pattern Recog.*, 2019, pp. 7479–7489.
- [245] G. Xavier and B. Yoshua, "Understanding the difficulty of training deep feedforward neural networks," in *Int. Conf. Artif. Intell. Stat.*, 2010, pp. 249–256.
- [246] Y. Xu, D. Xu, X. Hong, W. Ouyang, R. Ji, M. Xu, and G. Zhao, "Structured modeling of joint deep feature and prediction refinement for salient object detection," in *Int. Conf. Comput. Vis.*, 2019, pp. 3789–3798.
- [247] Y. Liu, Q. Zhang, D. Zhang, and J. Han, "Employing deep part-object relationships for salient object detection," in *Int. Conf. Comput. Vis.*, 2019, pp. 1232–1241.
- [248] Y. Zeng, Y. Zhuge, H. Lu, and L. Zhang, "Joint learning of saliency detection and weakly supervised semantic segmentation," in *Int. Conf. Comput. Vis.*, 2019, pp. 7223–7233.
- [249] J. Su, J. Li, Y. Zhang, C. Xia, and Y. Tian, "Selectivity or invariance: Boundary-aware salient object detection," in *Int. Conf. Comput. Vis.*, 2019, pp. 3799–3808.
- [250] J.-X. Zhao, J.-J. Liu, D.-P. Fan, Y. Cao, J. Yang, and M.-M. Cheng, "Egnet: Edge guidance network for salient object detection," in *Int. Conf. Comput. Vis.*, 2019, pp. 8779–8788.
- [251] S. Zhou, J. Wang, J. Zhang, L. Wang, D. Huang, S. Du, and N. Zheng, "Hierarchical u-shape attention network for salient object detection," *IEEE Trans. Image Process.*, vol. 29, pp. 8417–8428, 2020.
- [252] Y. Cai, L. Dai, H. Wang, L. Chen, and Y. Li, "A novel saliency detection algorithm based on adversarial learning model," *IEEE Trans. Image Process.*, vol. 29, pp. 4489–4504, 2020.
- [253] X. Li, D. Song, and Y. Dong, "Hierarchical feature fusion network for salient object detection," *IEEE Trans. Image Process.*, vol. 29, pp. 9165–9175, 2020.
- [254] J.-J. Liu, Q. Hou, and M.-M. Cheng, "Dynamic feature integration for simultaneous detection of salient object, edge, and skeleton," *IEEE Trans. Image Process.*, vol. 29, pp. 8652–8667, 2020.
- [255] M. Feng, H. Lu, and Y. Yu, "Residual learning for salient object detection," *IEEE Trans. Image Process.*, vol. 29, pp. 4696–4708, 2020.
- [256] L. Zhang, J. Wu, T. Wang, A. Borji, G. Wei, and H. Lu, "A multistage refinement network for salient object detection," *IEEE Trans. Image Process.*, vol. 29, pp. 3534–3545, 2020.
- [257] Y. Liu, J. Han, Q. Zhang, and C. Shan, "Deep salient object detection with contextual information guidance," *IEEE Trans. Image Process.*, vol. 29, pp. 360–374, 2020.
- [258] S. Chen, X. Tan, B. Wang, H. Lu, X. Hu, and Y. Fu, "Reverse attention-based residual network for salient object detection," *IEEE Trans. Image Process.*, vol. 29, pp. 3763–3776, 2020.
- [259] W. Wang, J. Shen, X. Dong, A. Borji, and R. Yang, "Inferring salient objects from human fixations," *IEEE Trans. Pattern Anal. Mach. Intell.*, vol. 42, no. 8, pp. 1913–1927, 2020.
- [260] H. Li, G. Li, B. Yang, G. Chen, L. Lin, and Y. Yu, "Depthwise nonlocal module for fast salient object detection using a single thread," *IEEE Trans. Cybern.*, 2020.
- [261] J. Li, Z. Pan, Q. Liu, Y. Cui, and Y. Sun, "Complementarity-aware attention network for salient object detection," *IEEE Trans. Cybern.*, 2020.
- [262] H. Li, G. Li, and Y. Yu, "Rosa: Robust salient object detection against adversarial attacks," *IEEE Trans. Cybern.*, vol. 50, no. 11, pp. 4835–4847, 2019.
- [263] J. Long, E. Shelhamer, and T. Darrell, "Fully convolutional networks for semantic segmentation," in *IEEE Conf. Comput. Vis. Pattern Recog.*, 2015, pp. 3431–3440.
- [264] L. Wang, R. Chen, L. Zhu, H. Xie, and X. Li, "Deep sub-region network for salient object detection," *IEEE Trans. Circ. Syst. Video Technol.*, 2020.
- [265] Z. Tu, Y. Ma, C. Li, J. Tang, and B. Luo, "Edge-guided non-local fully convolutional network for salient object detection," *IEEE Trans. Circ. Syst. Video Technol.*, 2020.
- [266] X. Hu, C.-W. Fu, L. Zhu, T. Wang, and P.-A. Heng, "Sac-net: Spatial attenuation context for salient object detection," *IEEE Trans. Circ. Syst. Video Technol.*, 2020.
- [267] Q. Ren, S. Lu, J. Zhang, and R. Hu, "Salient object detection by fusing local and global contexts," *IEEE Trans. Multimedia*, 2020.
- [268] Z. Wu, S. Li, C. Chen, A. Hao, and H. Qin, "A deeper look at image salient object detection: Bi-stream network with a small training dataset," *IEEE Trans. Multimedia*, 2020.
- [269] J. Li, Z. Pan, Q. Liu, and Z. Wang, "Stacked u-shape network with channel-wise attention for salient object detection," *IEEE Trans. Multimedia*, 2020.
- [270] G. Ma, C. Chen, S. Li, C. Peng, A. Hao, and H. Qin, "Salient object detection via multiple instance joint re-learning," *IEEE Trans. Multimedia*, vol. 22, no. 2, pp. 324–336, 2020.
- [271] S. Mohammadi, M. Noori, A. Bahri, S. G. Majelan, and M. Havaei, "Cagnet: Content-aware guidance for salient object detection," *Pattern Recogn.*, vol. 103, p. 107303, 2020.
- [272] B. Zoph, V. Vasudevan, J. Shlens, and Q. V. Le, "Learning transferable architectures for scalable image recognition," in *IEEE Conf. Comput. Vis. Pattern Recog.*, 2018, pp. 8697–8710.
- [273] X. Qin, Z. Zhang, C. Huang, M. Dehghan, O. R. Zaiane, and M. Jagersand, "U2-net: Going deeper with nested u-structure for salient object detection," *Pattern Recogn.*, vol. 106, p. 107404, 2020.
- [274] C. Wang, S. Dong, X. Zhao, G. Papanastasiou, H. Zhang, and G. Yang, "Saliencygan: Deep learning semisupervised salient object detection in the fog of iot," *IEEE Trans. Industr. Inform.*, vol. 16, no. 4, pp. 2667–2676, 2020.
- [275] S. Song, H. Yu, Z. Miao, J. Fang, K. Zheng, C. Ma, and S. Wang, "Multi-spectral salient object detection by adversarial domain adaptation," in *AAAI Conf. Art. Intell.*, vol. 34, no. 07, 2020, pp. 12 023–12 030.
- [276] B. Wang, Q. Chen, M. Zhou, Z. Zhang, X. Jin, and K. Gai, "Progressive feature polishing network for salient object detection," in *AAAI Conf. Art. Intell.*, vol. 34, no. 07, 2020, pp. 12 128–12 135.
- [277] Z. Chen, Q. Xu, R. Cong, and Q. Huang, "Global context-aware progressive aggregation network for salient object detection," in *AAAI Conf. Art. Intell.*, vol. 34, no. 07, 2020, pp. 10 599–10 606.
- [278] J. Wei, S. Wang, and Q. Huang, "F<sup>3</sup>net: Fusion, feedback and focus for salient object detection," in *AAAI Conf. Art. Intell.*, vol. 34, no. 07, 2020, pp. 12 321–12 328.
- [279] J. Wei, S. Wang, Z. Wu, C. Su, Q. Huang, and Q. Tian, "Label decoupling framework for salient object detection," in *IEEE Conf. Comput. Vis. Pattern Recog.*, 2020, pp. 13 025–13 034.
- [280] H. Zhou, X. Xie, J.-H. Lai, Z. Chen, and L. Yang, "Interactive two-stream decoder for accurate and fast saliency detection," in *IEEE Conf. Comput. Vis. Pattern Recog.*, 2020, pp. 9141–9150.
- [281] Y. Pang, X. Zhao, L. Zhang, and H. Lu, "Multi-scale interactive network for salient object detection," in *IEEE Conf. Comput. Vis. Pattern Recog.*, 2020, pp. 9413–9422.
- [282] J. Zhang, J. Xie, and N. Barnes, "Learning noise-aware encoder-decoder from noisy labels by alternating back-propagation for saliency detection," in *Eur. Conf. Comput. Vis.*, 2020.

- [283] S.-H. Gao, Y.-Q. Tan, M.-M. Cheng, C. Lu, Y. Chen, and S. Yan, "Highly efficient salient object detection with 100k parameters," in *Eur. Conf. Comput. Vis.*, 2020, pp. 702–721.
- [284] X. Zhao, Y. Pang, L. Zhang, H. Lu, and L. Zhang, "Suppress and balance: A simple gated network for salient object detection," in *Eur. Conf. Comput. Vis.*, 2020, pp. 35–51.
- [285] Y. Liu, M.-M. Cheng, X. Zhang, G.-Y. Nie, and M. Wang, "Dna: Deeply-supervised nonlinear aggregation for salient object detection," *IEEE Trans. Cybern.*, 2021.
- [286] Z. Chen, H. Zhou, J. Lai, L. Yang, and X. Xie, "Contour-aware loss: Boundary-aware learning for salient object segmentation," *IEEE Trans. Image Process.*, vol. 30, pp. 431–443, 2020.
- [287] S. Zhou, J. Wang, L. Wang, J. Zhang, F. Wang, D. Huang, and N. Zheng, "Hierarchical and interactive refinement network for edge-preserving salient object detection," *IEEE Trans. Image Process.*, vol. 30, pp. 1–14, 2020.
- [288] S. Yu, B. Zhang, J. Xiao, and E. G. Lim, "Structure-consistent weakly supervised salient object detection with local saliency coherence," in *AAAI Conf. Art. Intell.*, 2021.
- [289] M. Ma, C. Xia, and J. Li, "Pyramidal feature shrinking for salient object detection," in *AAAI Conf. Art. Intell.*, 2021.
- [290] B. Xu, H. Liang, R. Liang, and P. Chen, "Locate globally, segment locally: A progressive architecture with knowledge review network for salient object detection," in *AAAI Conf. Art. Intell.*, 2021.
- [291] S.-H. Gao, M.-M. Cheng, K. Zhao, X.-Y. Zhang, M.-H. Yang, and P. Torr, "Res2net: A new multi-scale backbone architecture," *IEEE Trans. Pattern Anal. Mach. Intell.*, vol. 43, no. 2, pp. 652–662, 2021.
- [292] C. Szegedy, V. Vanhoucke, S. Ioffe, J. Shlens, and Z. Wojna, "Rethinking the inception architecture for computer vision," in *IEEE Conf. Comput. Vis. Pattern Recog.*, 2016, pp. 2818–2826.
- [293] K. K. Singh and Y. J. Lee, "Hide-and-seek: Forcing a network to be meticulous for weakly-supervised object and action localization," in *Int. Conf. Comput. Vis.*, 2017, pp. 3544–3553.
- [294] H. Zhang, M. Cisse, Y. N. Dauphin, and D. Lopez-Paz, "mixup: Beyond empirical risk minimization," in *Int. Conf. Learn. Represent.*, 2017.
- [295] Z. Feng, C. Xu, and D. Tao, "Self-supervised representation learning by rotation feature decoupling," in *IEEE Conf. Comput. Vis. Pattern Recog.*, 2019, pp. 10364–10374.
- [296] L. Xie, J. Wang, Z. Wei, M. Wang, and Q. Tian, "Disturblabel: Regularizing cnn on the loss layer," in *IEEE Conf. Comput. Vis. Pattern Recog.*, 2016, pp. 4753–4762.
- [297] T. Miyato, S.-i. Maeda, M. Koyama, K. Nakae, and S. Ishii, "Distributional smoothing with virtual adversarial training," in *Int. Conf. Learn. Represent.*, 2016.
- [298] S. Thulasidasan, G. Chennupati, J. Bilmes, T. Bhattacharya, and S. Michalak, "On mixup training: Improved calibration and predictive uncertainty for deep neural networks," in *Adv. Neural Inform. Process. Syst.*, 2019.
- [299] S. Wager, W. Fithian, S. Wang, and P. Liang, "Altitude training: Strong bounds for single-layer dropout," in *Adv. Neural Inform. Process. Syst.*, 2014, pp. 100–108.
- [300] J. C. Peterson, R. M. Battleday, T. L. Griffiths, and O. Russakovsky, "Human uncertainty makes classification more robust," in *Int. Conf. Comput. Vis.*, 2019, pp. 9617–9626.
- [301] Y. Li, G. Hu, Y. Wang, T. M. Hospedales, N. M. Oberton, and Y. Yang, "Differentiable automatic data augmentation," in *Eur. Conf. Comput. Vis.*, 2020, pp. 580–595.
- [302] E. D. Cubuk, B. Zoph, D. Mane, V. Vasudevan, and Q. V. Le, "Autoaugment: Learning augmentation strategies from data," in *IEEE Conf. Comput. Vis. Pattern Recog.*, 2019, pp. 113–123.
- [303] Y. Wei, J. Feng, X. Liang, M.-M. Cheng, Y. Zhao, and S. Yan, "Object region mining with adversarial erasing: A simple classification to semantic segmentation approach," in *IEEE Conf. Comput. Vis. Pattern Recog.*, 2017, pp. 1568–1576.
- [304] Z. Zhong, L. Zheng, G. Kang, S. Li, and Y. Yang, "Random erasing data augmentation," in *AAAI Conf. Art. Intell.*, vol. 34, no. 07, 2020, pp. 13001–13008.
- [305] Y.-T. Chang, Q. Wang, W.-C. Hung, R. Piramuthu, Y.-H. Tsai, and M.-H. Yang, "Mixup-cam: Weakly-supervised semantic segmentation via uncertainty regularization," in *Brit. Mach. Vis. Conf.*, 2020.
- [306] H. Guo, Y. Mao, and R. Zhang, "Mixup as locally linear out-of-manifold regularization," in *AAAI Conf. Art. Intell.*, vol. 33, 2019, pp. 3714–3722.
- [307] S. Gidaris, P. Singh, and N. Komodakis, "Unsupervised representation learning by predicting image rotations," in *Int. Conf. Learn. Represent.*, 2018.
- [308] X. Zhai, A. Oliver, A. Kolesnikov, and L. Beyer, "S4l: Self-supervised semi-supervised learning," in *Int. Conf. Comput. Vis.*, 2019, pp. 1476–1485.
- [309] X. Chen, S. Xie, and K. He, "An empirical study of training self-supervised visual transformers," *arXiv preprint arXiv:2104.02057*, 2021.
- [310] X. Wang, K. He, and A. Gupta, "Transitive invariance for self-supervised visual representation learning," in *Int. Conf. Comput. Vis.*, 2017, pp. 1329–1338.
- [311] K. He, H. Fan, Y. Wu, S. Xie, and R. Girshick, "Momentum contrast for unsupervised visual representation learning," in *IEEE Conf. Comput. Vis. Pattern Recog.*, 2020, pp. 9729–9738.
- [312] H. Caesar, J. Uijlings, and V. Ferrari, "Coco-stuff: Thing and stuff classes in context," in *IEEE Conf. Comput. Vis. Pattern Recog.*, 2018, pp. 1209–1218.
- [313] S. Lazebnik, C. Schmid, and J. Ponce, "A sparse texture representation using local affine regions," *IEEE Trans. Pattern Anal. Mach. Intell.*, vol. 27, no. 8, pp. 1265–1278, 2005.
- [314] T. Judd, F. Durand, and A. Torralba, "A benchmark of computational models of saliency to predict human fixations," in *MIT Technical Report*, 2012.
- [315] F. Perazzi, J. Pont-Tuset, B. McWilliams, L. Van Gool, M. Gross, and A. Sorkine-Hornung, "A benchmark dataset and evaluation methodology for video object segmentation," in *IEEE Conf. Comput. Vis. Pattern Recog.*, 2016, pp. 724–732.
- [316] Q. Hou, M.-M. Cheng, X. Hu, A. Borji, Z. Tu, and P. Torr, "Deeply supervised salient object detection with short connections," *IEEE Trans. Pattern Anal. Mach. Intell.*, vol. 41, no. 4, pp. 815–828, 2019.
- [317] L. Yuan, F. E. Tay, G. Li, T. Wang, and J. Feng, "Revisiting knowledge distillation via label smoothing regularization," in *IEEE Conf. Comput. Vis. Pattern Recog.*, 2020, pp. 3903–3911.
- [318] G. Hinton, O. Vinyals, and J. Dean, "Distilling the knowledge in a neural network," in *Adv. Neural Inform. Process. Syst. Worksh.*, 2015.
- [319] C.-B. Zhang, P.-T. Jiang, Q. Hou, Y. Wei, Q. Han, Z. Li, and M.-M. Cheng, "Delving deep into label smoothing," *arXiv preprint arXiv:2011.12562*, 2020.
- [320] C. Godard, O. Mac Aodha, and G. J. Brostow, "Unsupervised monocular depth estimation with left-right consistency," in *IEEE Conf. Comput. Vis. Pattern Recog.*, 2017, pp. 270–279.
- [321] Z. Wang, A. C. Bovik, H. R. Sheikh, and E. P. Simoncelli, "Image quality assessment: From error visibility to structural similarity," *IEEE Trans. Image Process.*, vol. 13, no. 4, pp. 600–612, 2004.
- [322] K. Fu, D.-P. Fan, G.-P. Ji, Q. Zhao, J. Shen, and C. Zhu, "Siamese network for rgb-d salient object detection and beyond," *IEEE Trans. Pattern Anal. Mach. Intell.*, 2021.
- [323] S. Goferman, L. Zelnik-Manor, and A. Tal, "Context-aware saliency detection," *IEEE Trans. Pattern Anal. Mach. Intell.*, vol. 34, no. 10, pp. 1915–1926, 2011.
- [324] X. Zhu, C. Tang, P. Wang, H. Xu, M. Wang, J. Chen, and J. Tian, "Saliency detection via affinity graph learning and weighted manifold ranking," *Neurocomputing*, vol. 312, pp. 239–250, 2018.
- [325] C. Tang, P. Wang, C. Zhang, and W. Li, "Salient object detection via weighted low rank matrix recovery," *IEEE Signal Process. Lett.*, vol. 24, no. 4, pp. 490–494, 2016.
- [326] X. Huang and Y. Zhang, "Water flow driven salient object detection at 180 fps," *Pattern Recog.*, vol. 76, pp. 95–107, 2018.
- [327] J. Zhang, D.-P. Fan, Y. Dai, S. Anwar, F. Saleh, S. Aliakbarian, and N. Barnes, "Uncertainty inspired rgb-d saliency detection," *IEEE Trans. Pattern Anal. Mach. Intell.*, 2021.
- [328] J. Zhang, D.-P. Fan, Y. Dai, S. Anwar, F. S. Saleh, T. Zhang, and N. Barnes, "Uc-net: uncertainty inspired rgb-d saliency detection via conditional variational autoencoders," in *IEEE Conf. Comput. Vis. Pattern Recog.*, 2020, pp. 8582–8591.
- [329] C. Guo, G. Pleiss, Y. Sun, and K. Q. Weinberger, "On calibration of modern neural networks," in *Int. Conf. Mach. Learn.*, 2017, pp. 1321–1330.
- [330] D.-P. Fan, G.-P. Ji, M.-M. Cheng, and L. Shao, "Concealed object detection," *IEEE Trans. Pattern Anal. Mach. Intell.*, 2021.
- [331] K. R. Cave, "Finding meaning in eye movements," *Nat. Hum. Behav.*, vol. 1, no. 10, pp. 709–710, 2017.
- [332] J. M. Henderson, T. R. Hayes, C. E. Peacock, and G. Rehrig, "Meaning and attentional guidance in scenes: A review of the meaning map approach," *Vision*, vol. 3, no. 2, p. 19, 2019.
- [333] J. M. Henderson and T. R. Hayes, "Meaning-based guidance of attention in scenes as revealed by meaning maps," *Nat. Hum. Behav.*, vol. 1, no. 10, pp. 743–747, 2017.
- [334] X. Tian, K. Xu, X. Yang, B. Yin, and R. W. Lau, "Weakly-supervised salient instance detection," in *Brit. Mach. Vis. Conf.*, 2020.

- [335] Y.-H. Wu, Y. Liu, L. Zhang, W. Gao, and M.-M. Cheng, "Regularized densely-connected pyramid network for salient instance segmentation," *IEEE Trans. Image Process.*, vol. 30, pp. 3897–3907, 2021.
- [336] Y. Liu, D. Zhang, Q. Zhang, and J. Han, "Part-object relational visual saliency," *IEEE Trans. Pattern Anal. Mach. Intell.*, 2021.
- [337] A. R. Zamir, A. Sax, W. Shen, L. J. Guibas, J. Malik, and S. Savarese, "Taskonomy: Disentangling task transfer learning," in *IEEE Conf. Comput. Vis. Pattern Recog.*, 2018, pp. 3712–3722.
- [338] A. Li, J. Zhang, Y. Lv, B. Liu, T. Zhang, and Y. Dai, "Uncertainty-aware joint salient object and camouflaged object detection," in *IEEE Conf. Comput. Vis. Pattern Recog.*, 2021.
- [339] M. Zhuge, D. Gao, D.-P. Fan, L. Jin, B. Chen, H. Zhou, M. Qiu, and L. Shao, "Kaleido-bert: Vision-language pre-training on fashion domain," in *IEEE Conf. Comput. Vis. Pattern Recog.*, 2021.
- [340] G. Wang, C. Chen, D.-P. Fan, A. Hao, and H. Qin, "From semantic categories to fixations: A novel weakly-supervised visual-auditory saliency detection approach," in *IEEE Conf. Comput. Vis. Pattern Recog.*, 2021.
- [341] D. V. Ruiz, B. A. Krinski, and E. Todt, "Ida: Improved data augmentation applied to salient object detection," in *2020 33rd SIBGRAPI Conference on Graphics, Patterns and Images (SIBGRAPI)*, 2020, pp. 210–217.
- [342] Y. Liu, X.-Y. Zhang, J.-W. Bian, L. Zhang, and M.-M. Cheng, "Samnet: Stereoscopically attentive multi-scale network for lightweight salient object detection," *IEEE Trans. Image Process.*, vol. 30, pp. 3804–3814, 2021.
- [343] D.-P. Fan, G.-P. Ji, X. Qin, and M.-M. Cheng, "Cognitive vision inspired object segmentation metric and loss function," *SCIENTIA SINICA Informationis*, 2020.
- [344] Y. Mao, J. Zhang, Z. Wan, Y. Dai, A. Li, Y. Lv, X. Tian, D.-P. Fan, and N. Barnes, "Transformer transforms salient object detection and camouflaged object detection," *arXiv preprint arXiv:2104.10127*, 2021.
- [345] N. Liu, N. Zhang, K. Wan, J. Han, and L. Shao, "Visual saliency transformer," *arXiv preprint arXiv:2104.12099*, 2021.
- [346] H. Zhang, Y. Zeng, H. Lu, L. Zhang, J. Li, and J. Qi, "Learning to detect salient object with multi-source weak supervision," *IEEE Trans. Pattern Anal. Mach. Intell.*, 2021.
- [347] X. Zhao, Y. Pang, L. Zhang, H. Lu, and X. Ruan, "Self-supervised representation learning for rgb-d salient object detection," *arXiv preprint arXiv:2101.12482*, 2021.
- [348] R. Deora, R. Sharma, and D. S. S. Raj, "Salient image matting," *arXiv preprint arXiv:2103.12337*, 2021.